26896

National Library of Canada / Bibliothèque nationale du Canada

CANADIAN THESES ON MICROFICHE / THÈSES CANADIENNES SUR MICROFICHE

NAME OF AUTHOR/*NOM DE L'AUTEUR* Richard Lawrence Raddatz

TITLE OF THESIS/*TITRE DE LA THÈSE* Late Spring Upslope Weather on the Canadian Western Plains: a Mesoscale Numerical Simulation

UNIVERSITY/*UNIVERSITÉ* U. of Alberta

DEGREE FOR WHICH THESIS WAS PRESENTED/*GRADE POUR LEQUEL CETTE THÈSE FUT PRÉSENTÉE* M. Sc.

YEAR THIS DEGREE CONFERRED/*ANNÉE D'OBTENTION DE CE GRADE* 1975

NAME OF SUPERVISOR/*NOM DU DIRECTEUR DE THÈSE* Dr. K. Hage

Permission is hereby granted to the NATIONAL LIBRARY OF CANADA to microfilm this thesis and to lend or sell copies of the film.

The author reserves other publication rights, and neither the thesis nor extensive extracts from it may be printed or otherwise reproduced without the author's written permission.

*L'autorisation est, par la présente, accordée à la BIBLIOTHÈQUE NATIONALE DU CANADA de microfilmer cette thèse et de prêter ou de vendre des exemplaires du film.*

*L'auteur se réserve les autres droits de publication; ni la thèse ni de longs extraits de celle-ci ne doivent être imprimés ou autrement reproduits sans l'autorisation écrite de l'auteur.*

DATED/*DATÉ* June 26/75 SIGNED/*SIGNÉ* Richard Raddatz

PERMANENT ADDRESS/*RÉSIDENCE FIXE* 1587 Rothesay St
Winnipeg, Man

NL-91 (3-74)

THE UNIVERSITY OF ALBERTA

# LATE SPRING UPSLOPE WEATHER ON THE CANADIAN WESTERN PLAINS: A MESOSCALE NUMERICAL SIMULATION

by

© RICHARD LAWRENCE RADDATZ

A THESIS

SUBMITTED TO THE FACULTY OF GRADUATE STUDIES AND RESEARCH

IN PARTIAL FULFILMENT OF THE REQUIREMENTS FOR THE DEGREE

OF MASTER OF SCIENCE

IN

METEOROLOGY

DEPARTMENT OF GEOGRAPHY

EDMONTON, ALBERTA

FALL, 1975

THE UNIVERSITY OF ALBERTA

FACULTY OF GRADUATE STUDIES AND RESEARCH

The undersigned certify that they have read, and recommend to the Faculty of Graduate Studies and Research, for acceptance, a thesis entitled "Late Spring Upslope Weather on the Canadian Western Plains: A Mesoscale Numerical Simulation", submitted by Richard Lawrence Raddatz in partial fulfilment of the requirements for the degree of Master of Science in Meteorology.

Keith W. Hage
Supervisor

Edward Rogowski

Peter Antonelli

Date JUNE 24, 1975

DEDICATED TO

*Sherry and Stacey*

## ABSTRACT

Arctic outbreaks over the Canadian Western Plains during the late spring period frequently take the form of a cold east-northeasterly flow over a warmer, sloping surface. A mesoscale numerical model is developed in an attempt to simulate such circulations. Following Lavoie (1972) the atmospheric structure of the cold air mass is represented by three layers: a constant flux layer in contact with the earth's surface, a well mixed planetary boundary layer capped by an inversion, and a deep stratum of overlying stable air. Averaging the set of governing primitive equations through the depth of the mixed layer yields predictive equations for the horizontal wind components, potential temperature, specific humidity, and the height of the inversion. Time dependent calculations are limited to this layer by parameterizing the interactions between the mixed layer and both the underlying and overlying layers. Precipitation from limited convective clouds, and latent heat within the layer are included in terms of mesoscale variables.

A 47.6 km by 47.6 km grid mesh of 1369 points covering the Canadian Prairie Provinces is used to represent the variables in the mesoscale. The governing equations are solved numerically with terrain influences, surface roughness, temperature variations, and moisture fluxes allowed to perturb the mixed layer from its initial conditions until resultant mesoscale boundary layer weather patterns evolve.

The mean spring topographic precipitation pattern was successfully reproduced by the simulated late spring upslope flow with limited convective precipitation. This indicates that late spring upslope weather is a contributing factor to the upward swing in precipitation amounts over the Canadian Western Plains during the spring period. Mesoscale planetary boundary-layer weather patterns appear to exert a dominant control over the location and intensity of perturbations in the spring precipitation pattern. The elimination of surface heating significantly reduced the area and intensity of the precipitation. A case study based on observed initial conditions showed that the model could reproduce a persistent limited convective precipitation pattern maintained by upslope flow and that a low-level trough exerts a marked influence on the location and the intensity of the precipitation.

## ACKNOWLEDGEMENTS

I wish to thank Dr. K. Hage and Dr. M. L. Khandekar for their expert guidance during the term of this study. Thanks are also due to Dr. E. Lozowski and Dr. P. Antonelli who along with Dr. K. Hage served on my examining committee.

I also wish to thank Laura Smith who typed the final draft of this study and special thanks are due my fellow students for their helpful advice.

This study was conducted while on Educational Leave from the Atmospheric Environment Service, Environment Canada.

TABLE OF CONTENTS


| | | | Page |
|---|---|---|---|
| DEDICATION | | | iv |
| ABSTRACT | | | v |
| ACKNOWLEDGEMENTS | | | vii |
| TABLE OF CONTENTS | | | viii |
| LIST OF TABLES | | | x |
| LIST OF FIGURES | | | xi |
| CHAPTER | | | |
| 1 | | INTRODUCTION | 1 |
| | 1.1 | Preliminary Comments | 1 |
| | 1.2 | Physical Geography | 3 |
| | 1.3 | Late Spring Upslope Weather | 5 |
| | 1.4 | Outline of the Study | 7 |
| 2 | | THE MODEL | 9 |
| | 2.1 | Treatment of the Planetary Boundary Layer | 9 |
| | 2.2 | Thermal Structure Assumed in the Model Atmosphere | 10 |
| | 2.3 | Mesoscale Phenomena | 12 |
| | 2.4 | Governing Equations | 12 |
| 3 | | METHOD OF SOLUTION | 25 |
| | 3.1 | Numerical Technique | 25 |
| | 3.2 | Numerical Procedure | 27 |
| | 3.3 | Grid Domain, Topography and Drag Coefficients | 29 |

| CHAPTER | | | Page |
|---|---|---|---|
| 4 | | EXPERIMENTAL DESIGN, INITIALIZATION AND RESULTS . | 34 |
| | 4.1 | Introductory Comments . . . . . | 34 |
| | 4.2 | Simulation of Typical Late Spring Upslope Weather . . . . . | 35 |
| | 4.3 | A Sensitivity Experiment . . . . . | 56 |
| | 4.4 | Simulation of an Observed PBL Weather Pattern . . . . . | 58 |
| 5 | | SUMMARY AND CONCLUSIONS . . . . . | 76 |
| BIBLIOGRAPHY . . . . . | | | 79 |
| APPENDIX: BUILDING THE MODEL ATMOSPHERE . . . . . | | | 83 |

LIST OF TABLES


| Table | | Page |
|---|---|---|
| 1 | Extreme vertical velocities - Manitoba Escarpment | 48 |
| 2 | Extreme vertical velocities - other upland areas | 49 |
| 3 | Inversion deformations | 51 |
| 4 | Low-level wind profiles - April 26, 1969 | 70 |
| 5 | Inversion base height and mixed-layer winds | 75 |

LIST OF FIGURES


| Figure | Description | Page |
|---|---|---|
| 1 | Streamlines of the surface resultant winds in May (adapted from Bryson, 1966) | 2 |
| 2 | Topographic map of the Prairie Provinces (after Longley, 1972) | 4 |
| 3 | Thermal structure assumed in the model atmosphere (after Lavoie, 1972, 1974) | 11 |
| 4 | Relationship between precipitation rate and cloud depth | 19 |
| 5 | Grid domain | 30 |
| 6 | Typical low-level tephigram | 38 |
| 7 | Mean March to May precipitation (after Longley, 1972) | 42 |
| 8 | Mean topographic precipitation pattern (adapted from Longley, 1972) | 43 |
| 9 | Simulated topographic precipitation pattern | 45 |
| 10 | Simulated vertical velocity pattern | 46 |
| 11 | Simulated inversion deformation pattern | 50 |
| 12 | Vertical velocity-topography cross-section | 53 |
| 13 | Inversion deformation-topography ross-section | 54 |
| 14 | Precipitation-topography cross-section | 55 |
| 15 | Simulated inversion deformation pattern, $C_H = 0$ | 57 |

| Figure | | Page |
|---|---|---|
| 16 | Simulated precipitation pattern, $C_H = 0$ | 59 |
| 17 | Surface analysis 261200 GMT, April 1969 | 61 |
| 18 | 700 mb analysis 261200 GMT, April 1969 | 62 |
| 19 | 500 mb analysis 261200 GMT, April 1969 | 63 |
| 20 | Tephigrams - The Pas | 66 |
| 21 | Tephigrams - Fort Smith | 67 |
| 22 | Tephigrams - Edmonton | 68 |
| 23 | Tephigrams - Glasgow | 69 |
| 24 | Precipitation pattern - April 26, 1969 | 71 |
| 25 | Simulated precipitation pattern - April 26, 1969 | 72 |
| 26 | Simulated vertical velocity pattern - April 26, 1969 | 74 |

# CHAPTER 1

# INTRODUCTION

## 1.1 Preliminary Comments

The numerical experiment described in this thesis represents an initial attempt to simulate quantitatively the temporal and spatial evolution of mesoscale boundary-layer weather patterns resulting from the interaction of an east-northeasterly circulation of arctic air with the warmer, sloping Canadian Western Plains during the late spring period.

For Canada's Prairie Provinces, spring may be defined as the period March through May (Longley, 1972). However, spring is a complicated season showing significant variations in both time and space. Snow generally covers the entire region in early March; the snow line moves progressively northeastward pushing north of the Prairie Provinces by late May (McKay and Thompson, 1968). Climatic records indicate that spring is a time of increasing cloudiness, precipitation and wind speeds (Longley, 1972). Fig. 1 shows that it is also characterized by a mean east-northeasterly surface flow over all but the western areas (Bryson, 1966).

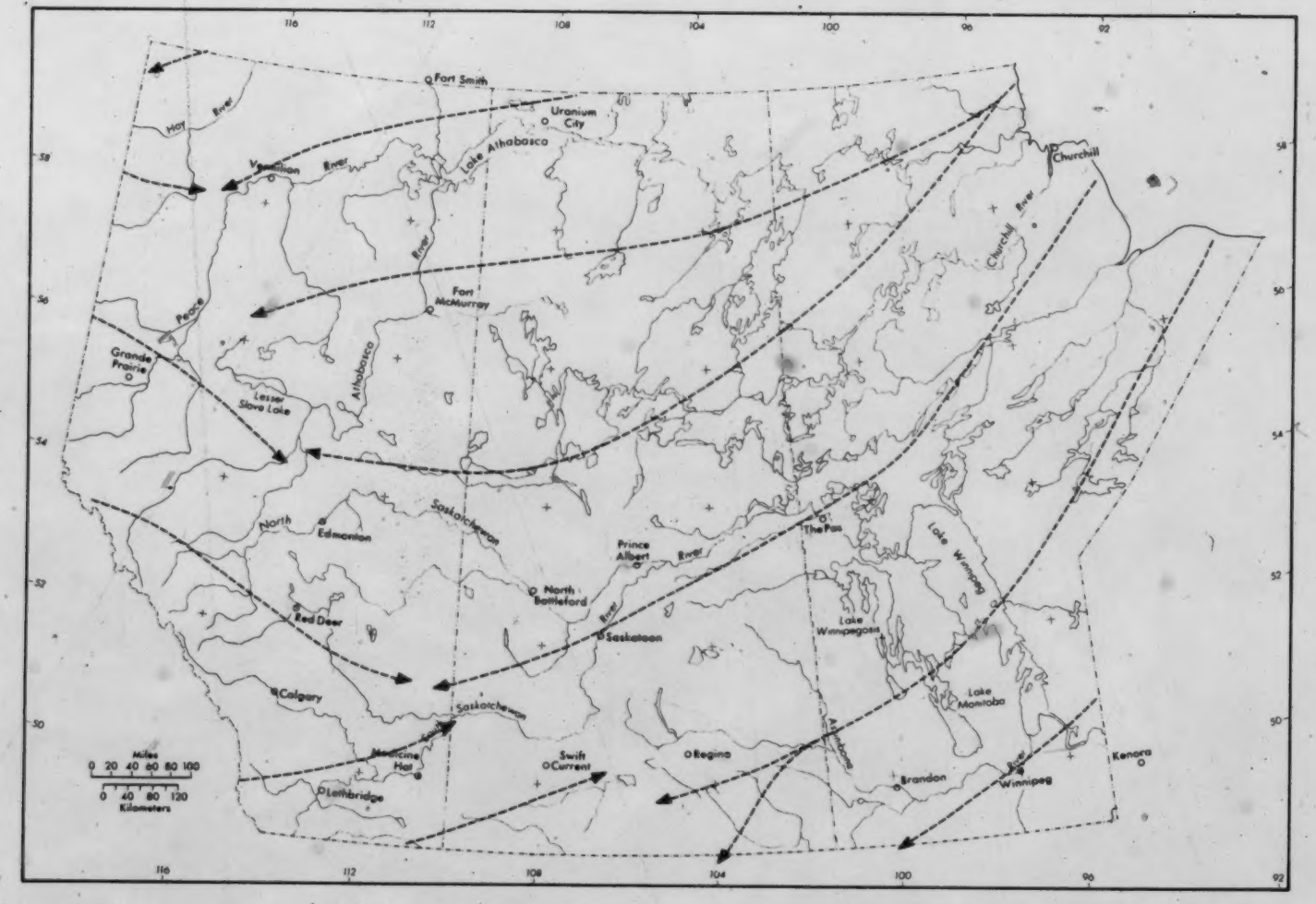


Fig. 1. Streamlines of the surface resultant winds in May (adapted from Bryson, 1966).

Late spring, usually late April or May, is the period when the northeast portion of the Prairie Provinces (the Canadian Shield portion) experiences rapid snow melt, and the Western Plains are snow free. Although the 'wet land surface period' on the plains may be quite short, and little or no vegetative growth is underway to supply moisture through transpiration, some water-vapour sources are provided by the numerous ponds and sloughs which have been filled by the snow-melt runoff. These small water bodies are usually very shallow, and they warm rapidly along with the snow-free land surface. A major moisture source is provided by snow melt on the Canadian Shield.

Arctic air sweeping down over the Prairie Provinces from the east-northeast encounters a relatively warm surface. This readily encourages evaporation as well as vertical fluxes of momentum and heat. Thus, spring's progression across this region, interrupted by arctic outbreaks, provides a complicated yet fascinating period for study.

## 1.2 Physical Geography

For the purpose of this study the Western Plains is defined as the region between the Canadian Shield and the Rockies. The eastern boundary extends from the southeast corner of Manitoba through Lake Winnipeg, and its northern limit is roughly along a line running from northern Lake Winnipeg to Fort McMurray then eastward to the British Columbia-Alberta border between the Hay and Peace Rivers (Fig. 2).

The most general feature of the relief of the Prairie Provinces is the westward upslope from the Hudson Bay lowlands in

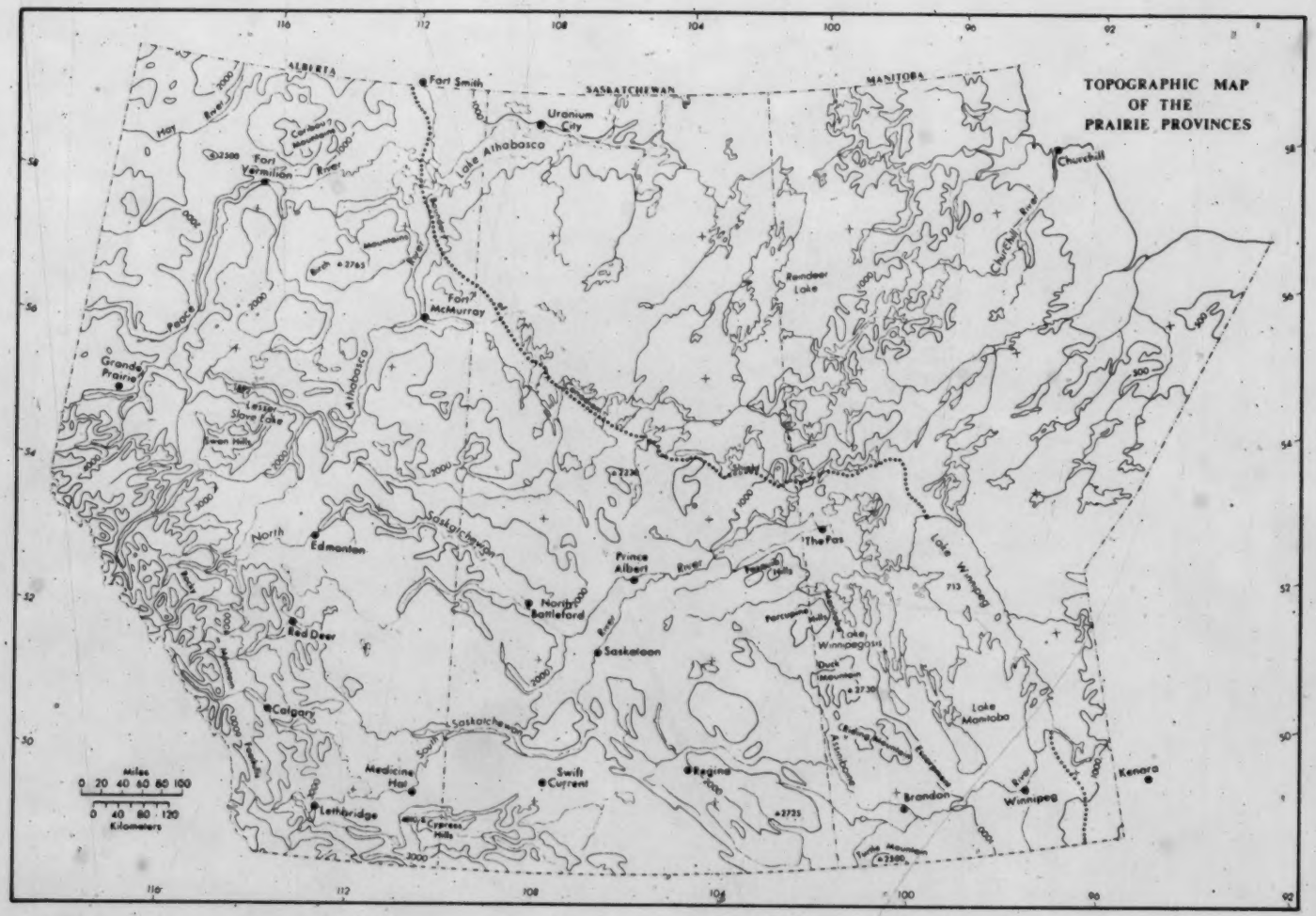


Fig. 2. Topographic map of the Prairie Provinces (after Longley, 1972).

the east to the Rockies in the west (Fig. 2). Within the plains region the topography is by no means uniform. Many lakes, ponds and sloughs occupy depressions in the landscape. Upland areas are found throughout the region. The most notable is the Manitoba escarpment including the Pasquia (2700 ft), Porcupine (2600 ft), Duck (2700 ft), Riding (2300 ft), and Turtle (2500 ft) tablelands. The Cypress Hills in southeastern Alberta and southwestern Saskatchewan rise to 4800 ft or over 2000 ft above the surrounding plains. Alberta has a number of other upland areas such as the Swan Hills (3800 ft) south of Lesser Slave Lake and the Birch Mountains (2800 ft) northwest of Fort McMurray.

## 1.3 Late Spring Upslope Weather

Late spring on the Western Plains is often dulled by extensive strata of limited convective clouds (stratocumulus). Cool, moderately moist winds gust out of the east-northeast and the ground is dampened by light drizzle showers, not infrequently mixed with snow. This type of weather is not only unpleasant for those trying to extend the short summer recreation period, but also has severe economic implications. In an area where agriculture is still the major industry, the grey clouds, blocking out the sun, retard surface drying and the precipitation further moistens the earth. This tends to keep the farmers off the land during the critical spring sowing period. The extensive low cloud also causes concern to those whose interests are in aviation.

Climatological charts (Longley, 1972) indicate that spring is characterized by increasing cloudiness and precipitation. Most certainly one of the contributing factors is the occurrence of late spring upslope weather. The term upslope generally refers to a persistent, shallow, east-northeasterly circulation associated with outbreaks of arctic air moving up the gently rising slope of the Western Plains. In late spring, this is normally a relatively unstable situation. The cold air mass moving south-westward up the sloping plains is heated from below by contact with the snow-free ground. This often produces turbulent low-level winds, and extensive decks of limited convective clouds (stratocumulus) accompanied by light drizzle showers or snowflurries. Limited convective condensation forms generally imply that the atmosphere is characterized by an unstable stratification of limited depth which is topped by a marked stable stratum (Willet and Sanders, 1959). The air is moistened from below by: (1) the numerous lakes making up over half the area of a thawing Canadian Shield, including lakes Winnipeg, Manitoba, and Winnipegosis, which lie to the east of the Western Plains and (2) the large number of ponds and sloughs which dot the plains. The unstable air flow, readily available moisture, and the sloping terrain must certainly contribute to the increasing cloudiness and precipitation during this season of the year.

The synoptic situation which produces a persistent east-northeasterly flow across the Western Plains usually consists of an arctic high moving from the Great Bear Lake area towards Lake Superior in conjunction with a low (especially a cold low) moving across the

northern United States.

The streamlines of the mean surface winds for May (Fig. 1) show an east-northeasterly flow over all but the western areas. The maps for March and April show a similar flow pattern (Bryson, 1966). These are mean maps. The day-to-day situation often shows the arctic front in a trough just east of the Rocky Mountains, subjecting the entire Western Plains to an east-northeasterly flow.

Although the Western Plains are often said to be in the rain shadow of the Rocky Mountains, actually the Rockies, and the sloping terrain from the Hudson Bay lowlands to the foothills of the Rockies, increase rather than decrease precipitation over the plains during the spring period. This has been shown convincingly, at least for Alberta and southwestern Saskatchewan by Reinelt (1969). It is readily seen from the mean spring precipitation chart (Longley, 1972) that the foothills and upland areas receive appreciably more precipitation than the surrounding lowland areas. This lends support to the proposition that unstable upslope flow is a contributing factor to the increased spring precipitation.

## 1.4 Outline of the Study

This study uses a three layer numerical model to simulate the mesoscale boundary layer weather patterns induced by a moderately moist, cold, east-northeasterly flow moving up the relatively warm sloping Western Plains. Time-dependent calculations are limited to a single mixed layer by parameterizing the interactions of this layer with the underlying and overlying layers. The procedure is based on

the hypothesis (after Lavoie, 1972, 1974) that a single well-mixed layer may be used to represent many of the significant aspects of mesoscale boundary layer weather disturbances, and that these mesoscale boundary layer disturbances provide effective control over the location and intensity of convective activity.

The model's ability to simulate 'typical' late spring upslope weather was tested initially. The relative importance of surface heating compared to friction and terrain relief in the production of limited convective precipitation was evaluated by running the model while neglecting vertical eddy heat fluxes under otherwise identical meteorological conditions. A case study was used to determine the model's ability to handle situations based on observed initial conditions.

The details of this study are presented in the following four chapters. Chapter 2 outlines the governing equations, together with details of the model atmosphere. Chapter 3 contains a brief description of the numerical technique used in this study, along with a step-by-step outline of the numerical procedure. The experimental design, together with the various results, are explained in Chapter 4. A brief summary and conclusions make up Chapter 5.

# CHAPTER 2

# THE MODEL

## 2.1 Treatment of the Planetary Boundary Layer

Following Deardorff (1972), the planetary boundary layer (PBL) may be defined as the region of the atmosphere adjacent to the earth's surface where small-scale turbulence is induced by thermal convection and wind shear. Clark (1970) and Deardorff (1972) have suggested that there are two possible approaches available for the treatment of the PBL. One is to resolve the vertical structure of the lower atmosphere explicitly by placing several layers in the lowest 1 to 3 km. This usually involves (1) parameterization of fluxes at the surface $Z_o$ and (2) modelling the turbulent diffusion of properties above $Z_s$, the height of the lowest model level. A second approach is to parameterize all aspects of the PBL so that its structure does not explicitly come into the computations; $Z_s$ is set at a much greater height, say 1 km and part (2) is by-passed.

Frequently the PBL is divided into a constant-flux (Prandtl) layer in which the fluxes of heat, momentum and water vapour are considered constant (i.e., having the same magnitude as at the surface) reaching some 10 to 80 m, and a second higher layer in which the

fluxes generally decrease with height. Under the conditions described in Chapter 1, a well-mixed atmosphere is often present in the lowest 1 to 2 km of the cold air mass. Mixing is induced both thermally as a result of surface heating along the trajectory of the arctic air, and mechanically by moderate low-level winds. Thus, the analysis of the PBL may be simplified by assuming that overlying the constant-flux layer is a convective layer which is well-mixed. It is assumed that the mixed layer is capped by an inversion. This upper stable layer completes the atmospheric structure.

## 2.2 Thermal Structure Assumed in the Model Atmosphere

The atmosphere is assumed to consist of three layers defined by distinctive lapse rates of potential temperature (Fig. 3). The vertical thermal structure includes:

(a) a surface layer ($Z_o$ to $Z_s$) characterized by a super-adiabatic lapse rate giving rise to a condition of upward heat flux. The upper limit is set at 10 m, the anemometer level.

(b) a mixed layer ($Z_s$ to h) in which the horizontal wind velocity $\vec{V}$, the potential temperature $\theta$, and the specific humidity q are assumed homogeneous in the vertical. Its upper limit is defined by a first-order discontinuity in potential temperature. The depth of this layer varies locally in space and time as a result of several forcing factors including: (1) varying surface heat fluxes, (2) varying surface momentum fluxes, (3) terrain slope, and (4) the release of latent heat from precipitation.

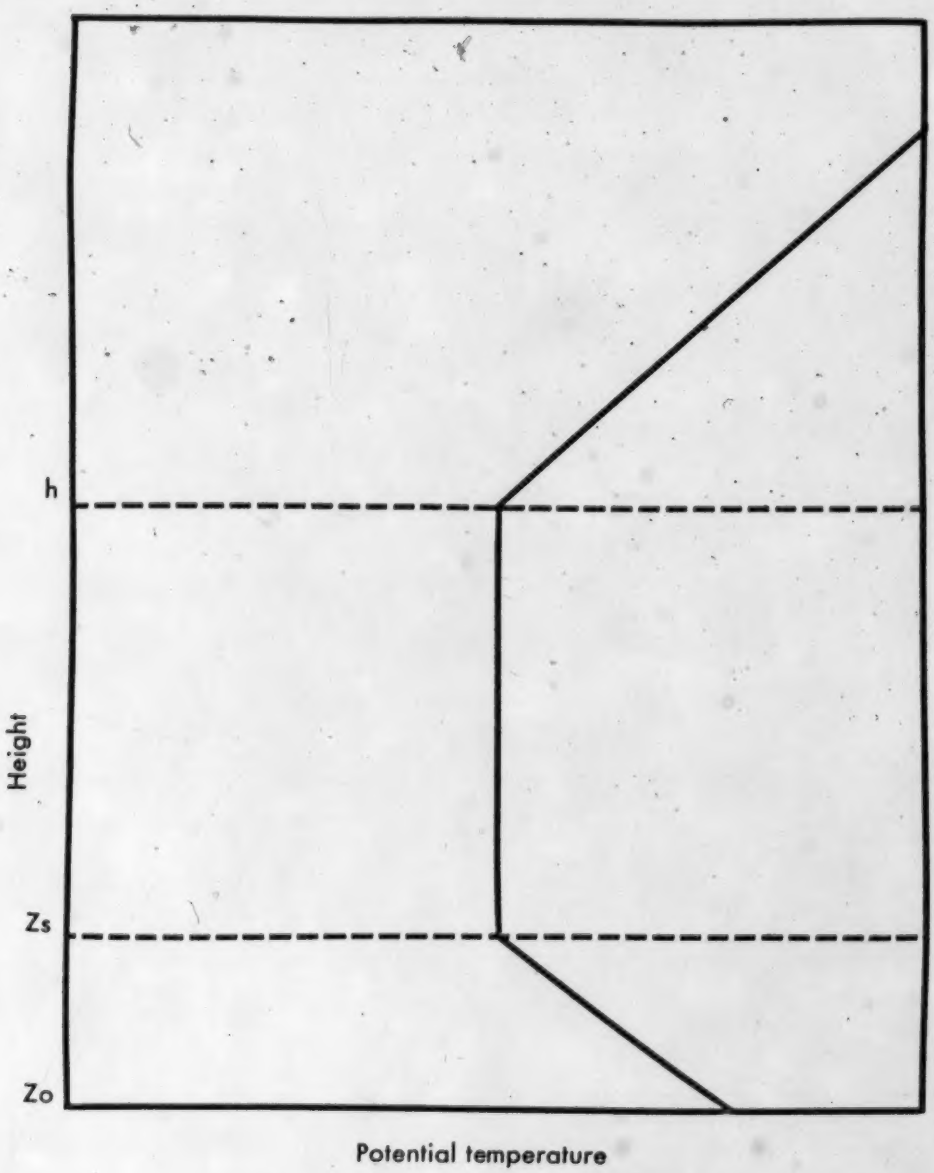


Fig. 3. Thermal structure assumed in the model atmosphere (after Lavoie, 1972, 1974).

(c) an upper layer ($Z>h$) consisting of a deep stable stratum with a constant lapse rate of potential temperature.

## 2.3 Mesoscale Phenomena

The model will be applied to weather systems whose characteristic dimensions are of the order of tens of kilometers in the horizontal and less than ten kilometers in the vertical. These phenomena fall within the scale of atmospheric motion usually referred to as mesoscale. Ogura (1963) points out that it is customary to assume hydrostatic balance for motions whose horizontal scale is much larger than the vertical scale. The assumption that the pressure field is determined by the density distribution alone, without reference to the field of motion, rules out the possibility of simulating individual convective clouds. However, it is hypothesized (after Lavoie, 1972, 1974) that the location and intensity of convective regions will be determined by the larger mesoscale weather patterns.

## 2.4 Governing Equation

The basic equations applied to a fluid parcel in the mixed layer (Lavoie, 1972, 1974) are

Horizontal momentum equation

$$\frac{d\vec{V}}{dt} = -\hat{k} \times f\vec{V} - \alpha \nabla p + \alpha \frac{\partial \vec{\tau}}{\partial Z} \qquad (1)$$

First and second laws of thermodynamics

$$\frac{d\theta}{dt} = -\frac{\alpha\theta}{C_p T}\frac{\partial Q}{\partial Z} + \frac{\alpha L \theta M'}{C_p T} \qquad (2)$$

Conservation of mass

$$\frac{1}{\alpha}\frac{d\alpha}{dt} = \nabla\cdot\vec{V} + \frac{\partial W}{\partial Z} \tag{3}$$

Conservation of water substance

$$\frac{dq}{dt} = -\alpha\frac{\partial E}{\partial Z} - \alpha M' \tag{4}$$

Definition of hydrostatic balance

$$\alpha\frac{\partial p}{\partial Z} = -g \tag{5}$$

Definition of potential temperature

$$\theta = \frac{\alpha}{R}\, p_*^{\kappa} / p^{\kappa-1} \tag{6}$$

Equation of state

$$p\alpha = RT \tag{7}$$

where the coordinate axes are chosen with the positive Z axis upward, the positive x axis to the east-northeast, and the positive y axis to the north-northwest, and where

- $\vec{\tau}$ is the vertical flux of horizontal momentum
- Q is the vertical flux of sensible heat
- M′ is the net condensation rate per unit volume
- E is the vertical flux of water vapour
- $p_*$ is a reference pressure of 1000 mb
- p is pressure
- $\vec{V}$ is the horizontal velocity vector

$q$ is specific humidity

$g$ is the acceleration due to gravity

$\alpha$ is the specific volume of dry air

$T$ is temperature

$W$ is vertical velocity

$\theta$ is potential temperature

$t$ is time

$f$ is the Coriolis parameter

$L$ is the latent heat of evaporation

$R$ is the gas constant for dry air

$C_p$ is the specific heat of dry air at constant pressure

$\kappa = R/C_p$

The behaviour of the mixed layer as a whole may be described by integrating from $Z_s$ to h, using the assumption of vertical homogeneity of horizontal wind velocity, potential temperature and specific humidity. Thus, the parcel derivatives of these quantities are independent of height.

(a) Horizontal momentum equation.

Averaging (1) through the mixed layer yields

$$\frac{d\vec{V}}{dt} = -\hat{k} \times f\vec{V} - \frac{1}{h - Z_s}\left[\int_{Z_s}^{h} \alpha \nabla p dZ - \alpha(\vec{\tau}_h - \vec{\tau}_s)\right] \qquad (8)$$

Assume that the momentun flux through the inversion surface $\vec{\tau}_h$ can be neglected. The flux through the lower boundary can be parameterized by means of the bulk aerodynamic method (Priestley, 1959).

$$\vec{\tau}_s = C_D \rho_s |\vec{V}| \vec{V} \qquad (9)$$

where $C_D$ is the drag coefficient and $\rho_s$ is the density at level $Z_s$.

The horizontal pressure gradient force can be calculated in terms of $\theta$ by eliminating $\alpha$ between (5) and (6).

$$\frac{\partial p^{\kappa}}{\partial Z} = -(g/C_p)\frac{p_*^{\kappa}}{\theta} \tag{10}$$

Assuming that pressure is known at some level H within the upper stable layer, integrate (10) from H down to an arbitrary level Z within the mixed layer.

$$p_Z = \left( p_H^{\kappa} - \frac{g}{C_p} p_*^{\kappa} \left[ - \frac{H - h}{\theta_H - \theta_h} \ln \frac{\theta_H}{\theta_h} + \frac{Z - h}{\theta} \right] \right)^{1/\kappa} \tag{11}$$

where $\theta_h$ is the potential temperature just above the inversion base, $\theta_H \neq \theta_h$ and $\theta_Z \equiv \theta$.

Taking the horizontal gradient of $p_Z$ multiplying by $-\alpha$ and approximating $\ln(\theta_H/\theta_h)$ by the first two terms of its Taylor series expansion (since $\theta_H/\theta_h$ is approximately one) yields

$$-\alpha \nabla p_Z = -\frac{\theta}{\theta_H}(\alpha \nabla p)_H + \frac{2g(H - h)}{\theta_H + \theta_h} \nabla \left( \frac{\theta_H + \theta_h}{2} \right)$$

$$+ \frac{g}{\theta_h} \left( \theta - \frac{\theta_h + \theta_H}{2} \right) \nabla h$$

$$+ \frac{g(h - Z)}{\theta} \nabla \theta \tag{12}$$

Because the final term in (12) is the only one that depends upon height, the vertical integration of (8) is readily accomplished. Letting $\vec{F} = \frac{\theta}{\theta_H}(\alpha \nabla p)_H$ represent the pressure gradient at level H

and $\bar{\theta} \equiv (\theta_h + \theta_H)/2$ represent the mean potential temperature of the layer $(H-h)$ and using (12) to re-write (8) gives

$$\frac{d\vec{V}}{dt} = -\hat{k} \times f\vec{V} - \vec{F}_H + g\frac{(H-h)}{\bar{\theta}}\nabla\bar{\theta} + \frac{g}{\theta_h}(\theta - \bar{\theta})\nabla h$$

$$+ g\frac{(h - Z_s)}{2\theta}\nabla\theta - \frac{C_D|\vec{V}|\vec{V}}{(h - Z_s)} \qquad (13)$$

In order to remove the critical dependence of the second and third terms of (13) upon the height of the undisturbed level H, the geostrophic wind shear in the upper stable layer is introduced in terms of the thermal gradient. The thermal wind equation is

$$-\frac{g}{\bar{\theta}}\nabla\bar{\theta} = f\hat{k} \times \frac{\partial\vec{V}_g}{\partial Z} \equiv f\vec{\psi} \qquad (14)$$

where $\vec{V}_g$ is the geostrophic wind in the upper layer and $\vec{\psi}$ is the rotated shear vector. If $\vec{\psi}$ can be considered essentially constant in the upper layer, then applying the definition of $\vec{F}$ at the initial height of the inversion

$$\vec{F}_H - \vec{F}_i = -(H - h_i)\, f\vec{\psi} \qquad (15)$$

or

$$\vec{F}_H + (H - h)\, f\vec{\psi} = \vec{F}_i + (h_i - h)\, f\vec{\psi} \qquad (16)$$

Substituting (16) into (13) eliminates reference to level H, except for $\frac{g}{\theta_h}(\theta - \bar{\theta})\nabla h$ which represents the restoring force due to the deformation of the inversion base. In order to retain the influence of the stable layer aloft, we take the effective level H to be the height of the inversion base h plus one half the difference

between the initial height $h_i$ of the inversion and the maximum altitude reached by the inversion surface as a result of the various topographical influences. That is, for the purpose of defining $\bar{\theta}$, let

$$H \equiv h + \frac{1}{2}(h_m - h_i) \tag{17}$$

where $h_m$ is the maximum disturbed height of the inversion surface. Then

$$\bar{\theta} = (\theta_h + \theta_H)/2 = \theta_h + \frac{\Gamma}{4}(h_m - h_i) \tag{18}$$

where $\Gamma$ is the vertical gradient of $\theta$ above the inversion. Using (14), (16), and (18) we may write (13) as

$$\frac{\partial \vec{V}}{\partial t} = -\vec{V}\cdot\nabla\vec{V} - \hat{k} \times f\vec{V} - \vec{F}_i - (h_i - h) f\vec{\psi}$$

$$+ \frac{g}{\theta_h}\left(\theta - \theta_h - \frac{\Gamma}{4}(h_m - h_i)\right)\nabla h$$

$$+ \frac{g}{\theta}(h - Z_s)\nabla\theta - \frac{C_D}{(h - Z_s)}|\vec{V}|\vec{V} \tag{19}$$

The time-dependent variables are $\vec{V}$, h and $\theta$.

(b) Potential temperature equation

Averaging (2) through the mixed layer and assuming $\left(\frac{\bar{\alpha}}{T}\right) = \frac{\bar{\alpha}}{\bar{T}}$ yields

$$\frac{\partial \theta}{\partial t} = -\vec{V}\cdot\nabla\theta - \frac{\theta\bar{\alpha}}{C_p\bar{T}}\frac{1}{(h - Z_s)}(Q_h - Q_s)$$

$$+ \frac{L\theta\bar{\alpha}}{C_p(h - Z_s)\bar{T}} M \tag{20}$$

where $\bar{\alpha}$ and $\bar{T}$ are the mean values for the layer. $Q_h$ is the heat flux through the inversion (neglected). $Q_s$ is the heat flux at the lower boundary (Priestley, 1959)

$$Q_s = C_p \rho_s C_H |\vec{V}| (\theta_o - \theta) \qquad (21)$$

where $C_H$ is the sensible heat transfer coefficient and $\theta_o$ is the potential temperature at ground level. M is the total rate of production of particles of precipitation size in terms of mass of water per unit area by limited convective clouds in the mixed layer or, alternatively, the local precipitation rate. The pertinent parameters are taken to be (1) the depth of the cloud given by the difference between the mean cloud-top height, that is, the height of the inversion base and the lifting condensation level, or the level to which unsaturated air would have to be raised dry adiabatically to produce condensation (cloud base) and (2) the mesoscale field of vertical velocities near cloud base. The precipitation rate may be represented by

$$M = (\varepsilon W_{CB} + 1) N \text{ mm hr}^{-1} \qquad (22)$$

where $N = a(D - k)^2$ is a representation of the precipitation from limited convective clouds in the absence of mesoscale vertical velocities (Fig. 4). The depth of the cloud D must exceed k kilometers before precipitation is generated and the precipitation rate increases more and more rapidly with increasing cloud depth. Observations of mid-latitude layer clouds by Mason and Howorth (1952) and, more recently, by Stewart (1964), indicate that a cloud must be 400 to 500 m

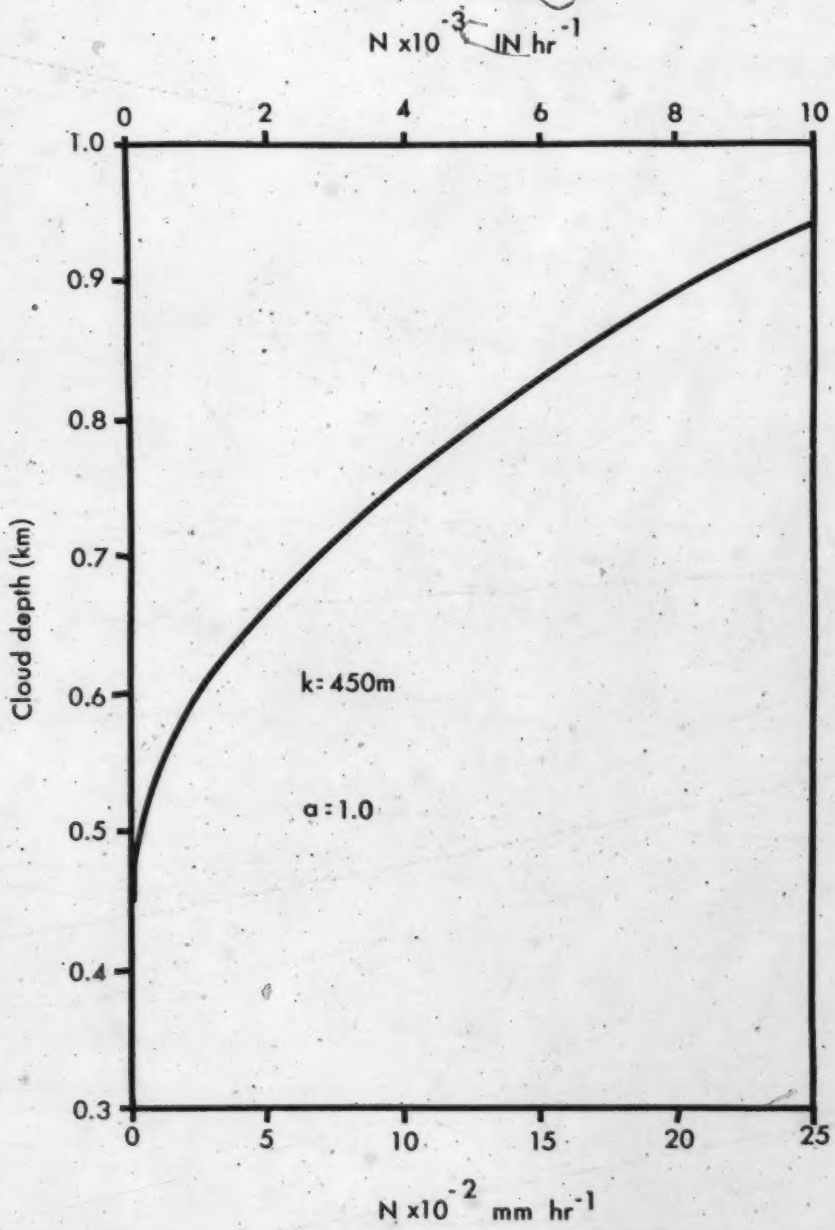


Fig. 4. Relationship between precipitation rate and cloud depth.

thick for precipitation to reach the ground. Therefore, k was set at 450 m. Parameter a is a measure of the efficiency of production of precipitation within the cloud; it was arbitrarily set to 1.0. $W_{CB}$ (cm $sec^{-1}$) is the mesoscale vertical velocity at cloud base. The parameter $\varepsilon$ was set equal to 0.5 $cm^{-1}$ sec so that mesoscale subsidence of 2 cm $sec^{-1}$ or more is sufficient to prevent precipitation.

The prognostic equation for $\theta$ becomes

$$\frac{\partial \theta}{\partial t} = - \vec{V} \cdot \nabla \theta + \frac{C_H}{(h - Z_s)} |\vec{V}| (\theta_o - \theta)$$

$$+ \frac{L \theta \bar{\alpha}}{C_p \bar{T}} \frac{M}{(h - Z_s)} \qquad (23)$$

(c) Mass continuity equation

Averaging (3) through the depth of the mixed layer yields

$$\overline{\frac{1}{\alpha} \frac{d\alpha}{dt}} = \nabla \cdot \vec{V} + \frac{W_h - W_s}{(h - Z_s)} \qquad (24)$$

The most significant contribution to the change in $\alpha$ of an air parcel is due to vertical motion

$$\overline{\frac{1}{\alpha} \frac{d\alpha}{dt}} \simeq \frac{g}{c^2} W \qquad (25)$$

where c is the isothermal speed of sound. Averaging (25) through the mixed layer gives

$$\overline{\frac{1}{\alpha} \frac{d\alpha}{dt}} \simeq \frac{g}{2c^2} (W_h + W_s) \qquad (26)$$

Using (25) and (26)

$$W_h = \left( W_s \left(1 + g(h - Z_s)/2c^2\right) - (h - Z_s)\nabla\cdot\vec{V} \right) \times \left[ 1 - g \frac{(h - Z_s)}{2c^2} \right]^{-1} \qquad (27)$$

where $W_s$ is the vertical velocity through $Z_s$ which can be taken to be entirely due to the sloping terrain

$$W_s = \vec{V}\cdot\nabla Z_o \qquad (28)$$

Assuming that the fluid surface at the top of the mixed layer can be considered to be a material surface, then

$$\frac{dh}{dt} = W_h \qquad (29)$$

In order to prevent the development of a superadiabatic layer at the top of the mixed layer when the inversion is wiped out by heating from below equation (29) is modified as follows

$$\frac{dh}{dt} = W_h + \left( \frac{1}{\Gamma} \frac{\partial\theta}{\partial t} \right)_{\theta=\theta_h}$$

where $\Gamma$ is the lapse rate of potential temperature in the upper layer and $\frac{1}{\Gamma}\frac{\partial\theta}{\partial t}$ is the rate of increase in the height of the top of the mixed layer that will maintain a first order discontinuity in $\theta$ at level h (included only when $\theta=\theta_h$).

The prognostic equation for h becomes

$$\frac{\partial h}{\partial t} = - \vec{V}\cdot\nabla h + W_h + \left( \frac{1}{\Gamma} \frac{\partial \theta}{\partial t} \right)_{\theta=\theta_h} \tag{30}$$

(d) Moisture continuity equation

Vertical integration of (4) yields

$$\frac{dq}{dt} = - \frac{\bar{\alpha}}{(h - Z_s)} (E_h - E_s) - \frac{\bar{\alpha} M}{(h - Z_s)} \tag{31}$$

Parameterizing the moisture flux through the lower boundary

$$E_s = \rho_s C_E |\vec{V}| (q_o - q) \tag{32}$$

and retaining the moisture flux through the top of the mixed layer because inversions generally display dry air aloft

$$E_h = \rho_h \beta |W_h| (q - q_h) \tag{33}$$

where $\beta$ is an arbitrary parameter (0.5) and $q_h$ is the specific humidity just above the inversion base.

The prognostic equation for q becomes

$$\frac{\partial q}{\partial t} = - \vec{V}\cdot\nabla q + \frac{C_E |\vec{V}|}{(h - Z_s)} (q_o - q)$$

$$= - \frac{\beta |W_h|}{(h - Z_s)} (q - q_h) - \frac{\bar{\alpha} M}{(h - Z_s)} \tag{34}$$

where M is given by (22) and $W_h$ by (27).

(e) The complete set of prognostic equations

$$\frac{\partial \vec{V}}{\partial t} = - \vec{V}\cdot\nabla\vec{V} - \hat{k} \times f\vec{V} - \vec{F}_i - (h_i - h) f\vec{\psi}$$

$$+ \frac{g}{\theta_h}\left(\theta - \theta_h - \frac{\Gamma}{4}(h_m - h_i)\right)\nabla h$$

$$+ \frac{g}{\theta}(h - Z_s)\nabla\theta - \frac{C_D}{(h - Z_s)}|\vec{V}|\vec{V} \qquad (19)$$

$$\frac{\partial \theta}{\partial t} = - \vec{V}\cdot\nabla\theta + \frac{C_H}{(h - Z_s)}|\vec{V}|(\theta_o - \theta)$$

$$+ \frac{L\theta\bar{\alpha}}{C_p\bar{T}} \frac{M}{(h - Z_s)} \qquad (23)$$

$$\frac{\partial h}{\partial t} = - \vec{V}\cdot\nabla h + W_h + \left(\frac{1}{\Gamma}\frac{\partial \theta}{\partial t}\right)_{\theta=\theta_h} \qquad (30)$$

$$\frac{\partial q}{\partial t} = - \vec{V}\cdot\nabla q + \frac{C_E|\vec{V}|}{(h - Z_s)}(q_o - q)$$

$$- \frac{\beta|W_h|}{(h - Z_s)}(q - q_h) - \frac{\bar{\alpha}M}{(h - Z_s)} \qquad (34)$$

In employing the above set of prognostic equations, the hypotheses and assumptions upon which they are based must be kept in mind. The guiding hypotheses for the simulation are: (a) that the model atmosphere is a reasonable representation of the actual atmospheric structure, (b) that a single well-mixed layer may be used to reproduce planetary boundary-layer weather patterns, and (c) that mesoscale PBL weather patterns control the location and intensity of convective activity. The acceptance of these hypotheses allows some simplifications of nature. The simplifications include: (a) the assumption of vertical homogeneity of $\vec{V}$, $\theta$ and $q$, (b) the use of the hydrostatic approximation, (c) the mesoscale parameterization of convective activity and (d) the limitation of time-dependent calculations to the mixed layer with parameterization of the interactions between this layer and both the underlying and overlying layers.

Although the above hypotheses and assumptions may be considered unduly restrictive, earlier work by Lavoie (1972, 1974) indicates that the model provides a useful first approximation to mesoscale boundary-layer weather patterns including convective precipitation induced by surface forcing factors. This justifies further applications of the single layer concept to those atmospheric situations where the original hypotheses and assumptions apply.

Improved parameterization of vertical fluxes, better vertical resolution by the introduction of more or other variables in the precipitation prediction technique are areas where changes may be needed.

# CHAPTER 3

# METHOD OF SOLUTION

## 3.1 Numerical Technique

Prognostic equations for $\vec{V}$, $\theta$, h, and q form a complete system of equations which may be solved numerically as an initial value problem with appropriate boundary conditions. The forward-upstream finite difference technique described by Lavoie (1972), and used earlier by Estoque (1962), Ogura (1962, 1963) and Orville (1964, 1965) among others, was chosen to represent the partial derivatives. The scheme consists of (1) a forward time step, (2) one-sided spatial differences evaluated upstream of each grid point for the advective terms, and (3) central differencing for non-advective terms. Haltiner (1971) has demonstrated that upstream differencing produces a damped solution. However, the damping characteristic of this technique should not significantly modify the results since the disturbances will be continually reinforced and are geographically fixed. Furthermore, the damping of short wavelengths should effectively prevent the nonlinear numerical instability that arises from aliasing of short waves. The accuracy of this scheme for simulating propagating waves in

comparison to other finite differencing techniques has been discussed by Molenkamp (1968). He indicates that it is less accurate than some alternate techniques; however, it has the advantage of requiring less computer time.

A 47.6 km by 47.6 km grid mesh of 1369 points was used to represent numerically the variables in the mesoscale. The choice of a time increment was somewhat empirical, because a linear computational stability analysis of the complete difference equations is very difficult. The increment $\Delta t$ was estimated simply from the stability criterion for the basic two dimensional advection equation. Therefore, the stability criterion is

$$c\Delta t/\Delta x < 2^{-\frac{1}{2}} \qquad \text{(Haltiner, 1972)}$$

where c is the phase speed of the fastest waves, $\Delta t$ is the time increment, and $\Delta x$ is the horizontal space increment. A time increment of 5 min. appeared to be acceptable because no evidence of instability showed up throughout the integration period.

Small-scale perturbations created by fast-moving gravity waves, boundary effects and truncation errors may, if left unchecked, 'blow-up' and obscure the meteorological phenomena. The growth of such spurious short waves was effectively controlled by explicit smoothing of the predicted fields after every fourth time step. The following smoothing operator was used to damp short waves (Asselin, 1966):

$$S(i,j) = A(i,j) + b/4(A(i-1,j) + A(i+1,j) + A(i,j-1) + A(i,j+1) - 4A(i,j))$$

where S(i,j) is the smoothed grid point value, A(i,j) is the grid

point value and b is the smoothing parameter set equal to +0.5. The predicted fields are then 'desmoothed' by applying the above operator a second time with b now equal to -0.5. This partially restores the amplitude of wavelengths which have been damped by the original smoothing. The response function of the smoothing and desmoothing operators is

$$R(k_i) = \left(\frac{1}{n}\right) \sum_{i=1}^{n} (1 - b + b \cos k_i \Delta x)$$

where $\Delta x$ = grid spacing, b = the smoothing parameter, n = the number of dimensions and $k_i$ is the wave number.

## 3.2 Numerical Procedure

The computational steps required for this numerical simulation are given below.

### 3.2.1 Initial Conditions

Wind, layer depth, potential temperature and specific humidity in the mixed layer are set uniform over the entire grid. The pressure gradient is calculated assuming level terrain without heat and moisture sources. Friction typical of a level land-water surface is included so that the wind vectors cross the isobars at a specified angle. The Coriolis parameter f is allowed to vary across the region.

The procedure of calculating the pressure from the wind field was followed because the numerical solution of the primitive equations is extremely sensitive to initial conditions. The primitive momentum equation equates acceleration to the resultant of Coriolis,

friction and pressure-gradient forces per unit mass. This resultant is normally about ten percent of the individual forces, so that observational errors or 'noise' due to microscale phenomena in the pressure or wind fields may be as large as the accelerations themselves. Such spurious accelerations create fictitious gravity waves whose amplitudes may be larger than those encountered in the real atmosphere (Thompson, 1961). This problem can be avoided by imposing the somewhat artificial condition of balance between the Coriolis, friction and the pressure-gradient forces at the initial time. In view of the fact that the wind may be considered the defining parameter for spring upslope weather, the pressure field is calculated from the wind field; this ensures a pressure field compatible with the initial wind field.

High frequency gravity waves in the initial wind and pressure fields are damped by applying the previously-defined smoothing and desmoothing operators.

### 3.2.2 Readjustment Process

At the start of integration, the surface is uncovered and the terrain relief is exposed. The momentum and heat fluxes proceed to alter the flow while, at the same time, vertical motions induced by the winds blowing against the sloping terrain begin to perturb the upper boundary of the mixed layer. The readjustment process proceeds as follows: (1) advance the horizontal wind components u and v to $t = \Delta t/2$, (2) use these forecast values of u and v midway through the first time interval to advance $\theta$, q, and h to $t = \Delta t$, (3) subsequent u and v steps are taken over $\Delta t$, but the wind continues to be evaluated at times midway through the interval over

which the other three fields are advanced. This procedure permits the maximum time step to be nearly double that required for linear computational stability with the non-staggered format (Lavoie, 1972). Integration is continued for six hours of model time to provide a sufficient interval for the $\vec{V}$, h, $\theta$ and q fields to respond to the various forcing factors. It was found that after six hours the rate of change of the dependent variables had become sufficiently small that a near steady-state solution may be assumed.

### 3.2.3 Boundary Conditions

The dependent variables are held constant at the inflow and side boundaries. At the outflow boundaries the value of the dependent variables are set equal, at each time step, to the values at the next grid point upstream.

## 3.3 Grid Domain, Topography and Drag Coefficients

### 3.3.1 Grid Domain

Figure 5 shows the area of interest and the grid domain. The grid, based on the standard 381 km northern hemispheric grid, consists of 37 rows and 37 columns. The spacing is equal to 47.6 km in the x and y directions, true at 60N latitude on a polar stereographic projection. The orientation of the grid is such that the x-axis is nearly parallel to the gradient of the terrain, with the Canadian Shield lying upstream of the Western Plains for an east-northeasterly flow. The Continental Divide provides a natural boundary to the southwest, while Hudson Bay serves a similar function

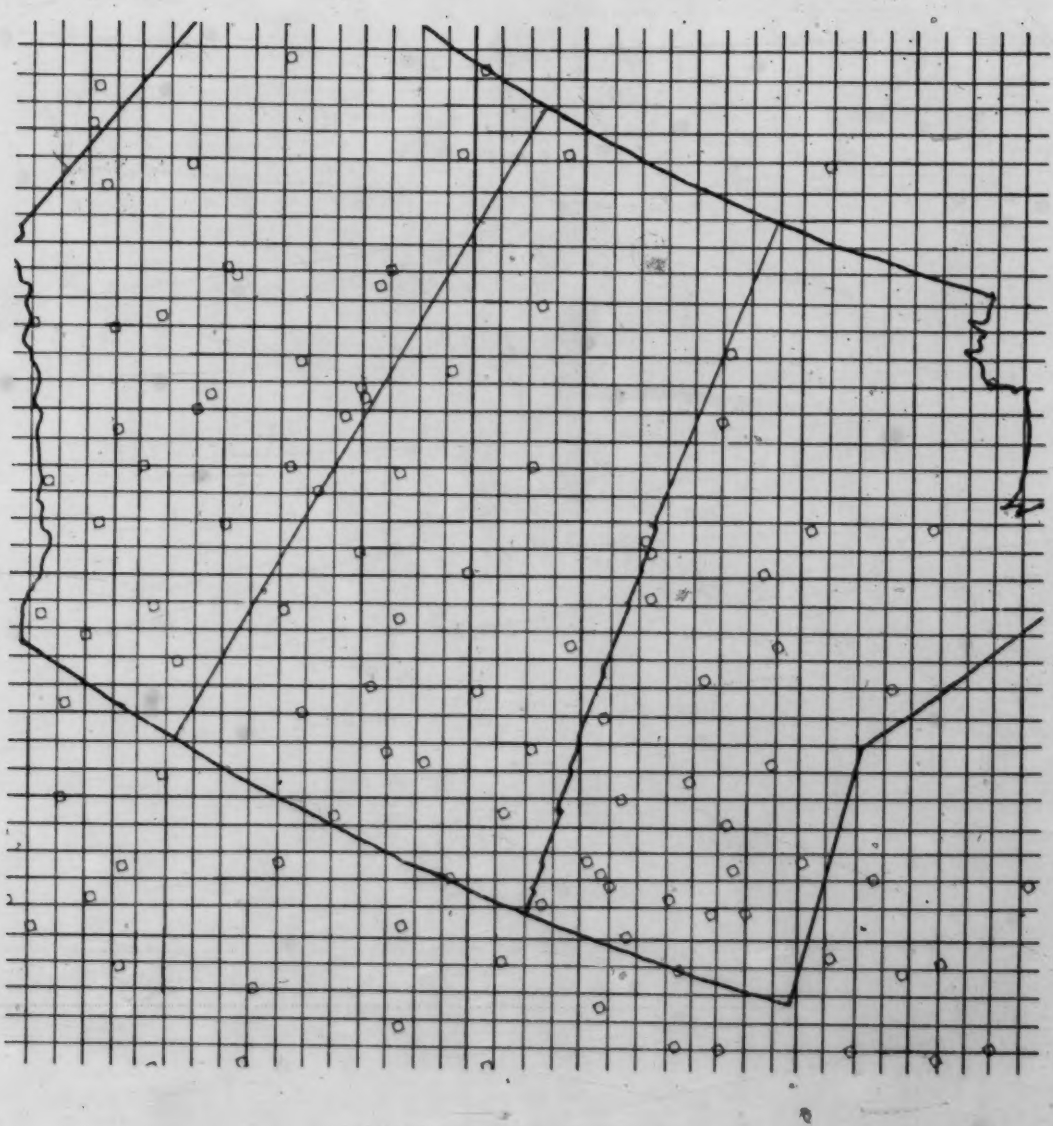


Fig. 5. Grid domain. (The outermost ring of intersections represents the grid boundary.)

to the northeast. The northwest and southeast edges of the grid were chosen to incorporate the maximum amount of the Canadian Western Plains.

### 3.3.2 Topography

The terrain elevation at each grid point was obtained from topographic maps[1] of scale 1:250,000. A large portion of these data had been abstracted previously by Charette (1971). The terrain grid-point values were smoothed using the same smoothing operator that was subsequently applied to the predicted fields. This provided a smoothed topographical field on the same scale as the atmospheric motion being considered.

### 3.3.3 Drag Coefficients

In order to include fluxes of momentum, sensible heat and moisture in the model, it is necessary to know the spacial distribution of $C_D$, the drag coefficient, $C_H$, the sensible heat transfer coefficient and $C_E$, the evaporation coefficient over the area of interest. It is also desirable to relate these coefficients to the horizontal wind speed and to atmospheric stability.

Following Cressman (1960), we discriminate between the drag coefficient over flat land or water (skin drag), and the drag due to terrain relief (terrain drag). The drag coefficient $C_D$ is considered to be made up of two partial drag coefficients $C_1$ and $C_2$, where $C_1$ is

---

[1] Topographic series produced and printed in Canada by the Surveys and Mapping Branch, Department of Energy, Mines and Resources, Government of Canada and in the United States by the Interior Geological Survey, Washington, D.C.

the skin drag and $C_2$ is the terrain drag coefficient. Values for $C_2$ for the standard 381 km northern hemispheric grid were supplied by Dr. Cressman of NOAA through G. R. Schram. These values were extended to the 47.6 km grid, a subset of the standard grid, by linear interpolation with minor subjective changes. Rather than using a constant value of $C_1$ as Cressman (1960) has done, an attempt was made to relate the skin drag coefficient to the horizontal wind speed (m $sec^{-1}$) using the following formula (Deacon and Webb, 1962):

$$C_1 = (1 + 0.7|\vec{V}|)0.001$$

Given the drag coefficient for the neutral atmosphere $C_{Dn}$ as a function of wind speed and terrain relief, we proceed to adjust these values according to atmospheric stability after Deardorff (1968). For the unstable case, which is the only one that applies in this simulation, the drag coefficient becomes:

$$C_D = (1 + (7/a) \text{ Log } (1 - aR_{ib}))C_{Dn}$$

where $a = 0.83\ C_{Dn}^{-0.62}$, and $R_{ib}$ is the bulk Richardson number, a measure of atmospheric stability.

$$R_{ib} = \frac{g}{T_v} \frac{Z}{|\vec{V}| - |\vec{V}_o|} \left( \theta - \theta_o + 0.61 \frac{C_E}{C_H} (q - q_o)T \right)$$

where Z is the height where $\vec{V}$, $\theta$ and q are known, g is the acceleration due to gravity, the subscript o refers to surface values with $|\vec{V}_o| = 0$ and $T_v$ is the virtual temperature, here assumed to be equal to T which is given by $(T_Z + T_o)/2$.

The sensible heat and water vapour transfer coefficients are obtained by assuming $C_H = C_E = C_D$ for the neutral case and then

adjusting the values of $C_H$ on the basis of stability after Deardorff (1968), while continuing to assume that $C_E = C_H$. Therefore, the heat and water vapour transfer coefficients become:

$$C_H = C_E = (1 + (11/c) \text{ Log } (1 - cR_{ib})) C_{Dn}$$

where $c = 0.25\ C_{Dn}^{-0.80}$.

The fields of drag coefficient and transfer coefficient grid-point values are smoothed using the previously defined smoothing and desmoothing operators. These values are assumed to remain constant during the integrating period.

# CHAPTER 4

## EXPERIMENTAL DESIGN, INITIALIZATION, AND RESULTS

### 4.1 Introductory Comments

It has been hypothesized after Lavoie (1972, 1974) that a single well-mixed layer may be used to represent many of the significant aspects of mesoscale boundary-layer weather disturbances and that these disturbances provide control over the location and intensity of convective activity. The present model has been designed to study the evolution of a well-mixed planetary boundary layer in response to several forcing factors including terrain relief, friction, surface heating and the release of latent heat accompanying the formation of precipitation. This represents an initial attempt to simulate quantitatively the temporal and spatial evolution of mesoscale atmospheric weather patterns resulting from the interaction of an east-northeasterly circulation of moderately moist arctic air with the relatively warm, sloping Canadian Western Plains during late spring.

Vertically homogeneous initial distributions of the dependent variables layer depth, wind, specific humidity and potential temperature were used. Detailed upstream topography was not delineated

initially, because there is little relief over the Canadian Shield. Friction was assumed to be the same over the whole grid so as to provide balanced flow with respect to the Shield at all grid points. At t = 0 the Western Plains was 'uncovered' with its topography, roughness differential, moisture sources and stronger surface heating. The readjustment procedure was followed at each grid point by means of equations (19), (23), (30), and (34) using the forward upstream numerical integration scheme. Integration was continued for six hours of model time to provide a sufficient interval for the PBL to respond to the various surface forcing factors. It was found that after six hours the rate of change of the dependent variables had become sufficiently small that a near steady state solution was achieved.

Lavoie (1972, 1974) has shown that the deformation of the inversion surface from its initial height is a useful guide to the intensity and distribution of mesoscale convective precipitation. Following Lavoie but on a scale nearly one order of magnitude larger than his, we proceed using the hypothesis that the atmospheric response on the mesoscale is dictated by the behaviour of the mixed layer as a whole with only secondary dependence on the detailed vertical structure.

## 4.2 Simulation of Typical Late Spring Upslope Weather

The most representative low-level flow conditions for late spring over the Canadian Western Plains are similar to the mean, for during the encompassing period, March through May, the average surface circulation persists out of the east-northeast for all but the western

regions (Bryson, 1966). Typical daytime values of atmospheric structure and low level flow were selected to test the ability of the model to simulate late spring upslope weather. The term upslope is usually applied to a shallow east-northeasterly circulation associated with outbreaks of arctic air masses over the Western Plains. Such easterlies are usually confined to the lowest 1 to 2 km of the atmosphere.

During the spring thaw period the surface of the Canadian Shield, which is normally over 50 percent water in the summer-time, probably approaches a true water or 'lake' surface with a temperature near 0C. Continental Arctic air (cA) is modified rapidly to a brand of air very similar in character to a winter cold maritime Arctic (cmA) air mass, with typical wet-bulb potential temperatures in the range $-5C < \theta_w < -1C$. This modified arctic air is usually referred to as transitional continental Arctic (tcA). The resulting unstable turbulent low-level flow, further perturbed by upslope and stronger surface heating upon reaching the Western Plains often produces extensive decks of limited convective clouds (stratocumulus). Precipitation will generally be light and intermittent and may take the form of drizzle or snow. The duration of these conditions may be several days.

At time $t = 0$ an east-northeasterly flow of arctic air, modified to tcA by interacting with the Shield, was assumed to cover the entire grid domain. The model air mass was horizontally uniform with the same vertical structure and low-level flow at all grid points. For $t > 0$ the topography was uncovered. As the integration proceeded

mesoscale weather patterns with areas of limited convective precipitation evolved due to spatial and temporal changes in the well-mixed boundary layer.

The 'undisturbed' air mass and surface parameters used to initialize the simulation of 'typical' late spring upslope weather are outlined below. Fig. 6 depicts the tcA sounding. The wet bulb potential temperature $\theta_w$ was taken to be -3C, the surface temperature $T_o$ was assumed to be 0C, and the inversion height h was set at 1.4 km, all in accordance with the previous discussion. The thermal structure of the model, the Normand principle (Normand, 1938), and the above values determined the surface dewpoint to be near -6.7C. The surface height of the Shield, $Z_o$, was set at 250 m above msl; detailed terrain was ignored at the initial time because there is little relief over the Shield. The vertical structure or representative sounding of the model atmosphere was then built up from surface values. This was done because a predictive role using actual data was envisaged in the model's future and it was felt desirable to build into the model the ability to use the wealth of surface data rather than the relatively scarce upper air data. The lapse rate of temperature was arbitrarily set at 10.2C $km^{-1}$ for the constant-flux layer from the surface $Z_o$ to the anemometer level $Z_s$, and a dry-adiabatic lapse rate of 9.8C $km^{-1}$ was required by the model atmosphere from $Z_s$ to h, the top of the well-mixed layer. A near isothermal layer was assumed above h. The superadiabatic surface layer ensured an initial upward heat flux. The lapse rate of dewpoint was set at 10.1C $km^{-1}$ from the surface to level h. This

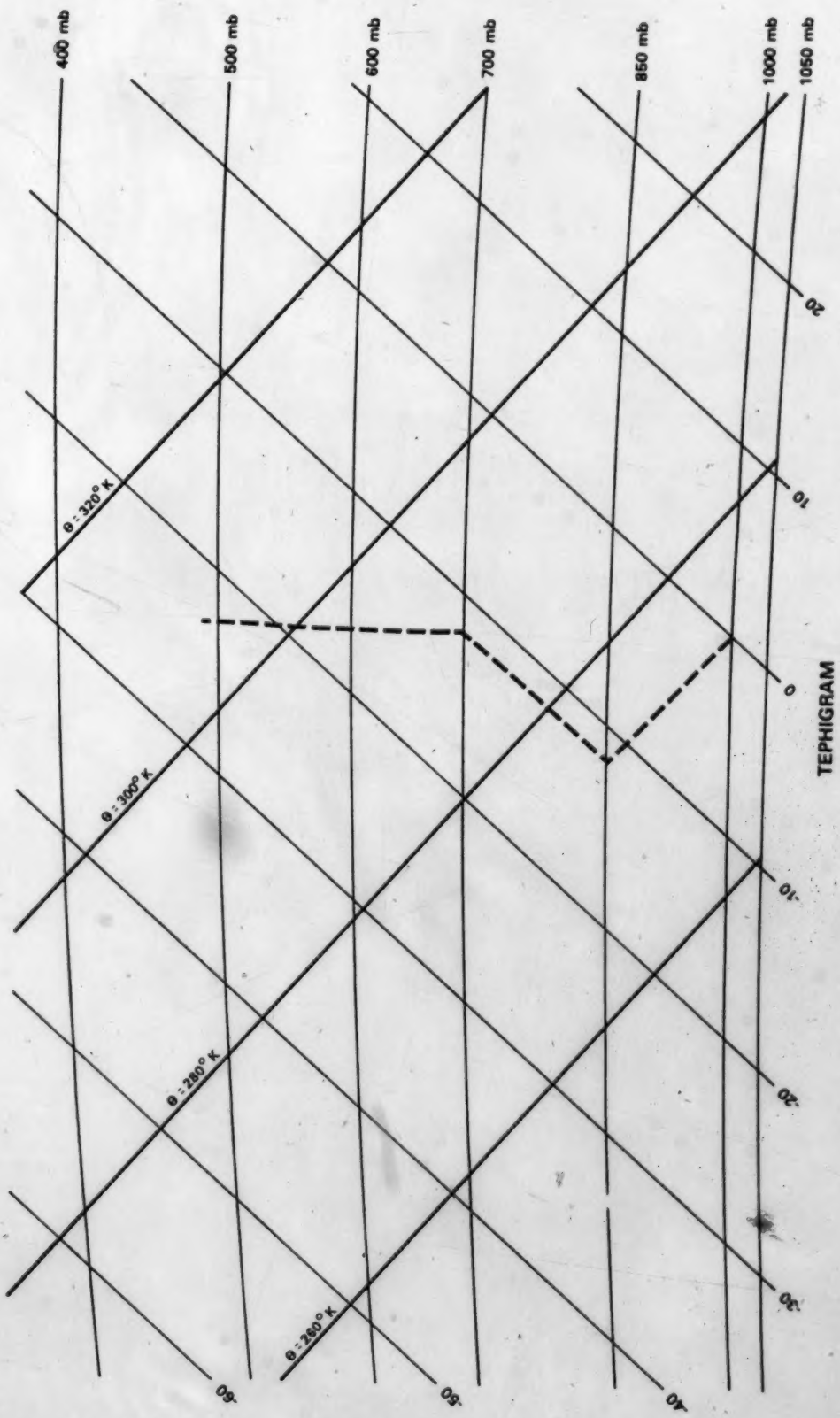


Fig. 6. 'Typical' low-level tephigram.

decrease which is slightly in excess of the decrease in temperature with height maintained a nearly constant $\theta_w$ value through the boundary layer and it also ensured an initial upward flux of moisture. The above values were then used to compute the model parameters of potential temperature and specific humidity at the various levels (see Appendix). The cloud base given by the lifting condensation level (LCL), or the level to which unsaturated air would have to be raised in a dry-adiabatic expansion to produce condensation, was assumed uniform throughout the air mass and was calculated as outlined in Pettersen (1956) (see Appendix).

The greater proportion of land to water surface on the Western Plains coupled with the earlier loss of snow cover allows the surface of the plains to heat under day-time conditions to a potential temperature in excess of the surface potential temperature $\theta_o$ on the Shield. An excess surface potential temperature $\theta_{o+}$ value of 4K was chosen to represent mid-day conditions on the plains. A transition area between the Shield and the plains was included with surface excess potential temperature taken to be $\theta_{o+}/2$.

Since vertical homogeneity of the horizontal wind was assumed, a representative mixed-layer wind was taken from the mean surface (anemometer level) streamline pattern for May given by Bryson (1966), Fig. 1. This is the mean flow. The periods of interest are those days when the discontinuity in the wind field lies just east of the Rockies subjecting the entire Western Plains area to an east-northeasterly flow. A horizontal wind from 075 degrees at 7 m $sec^{-1}$ was taken as representative of conditions over

the Shield. This was assumed to be the flow at all grid points initially. A detailed wind field was not included initially for two reasons: (a) it is impossible to obtain a horizontal wind field that has not already been influenced by topography and (b) using a uniform field avoided the problem of including real or fictitious lines of convergence or divergence at the initial time which might mask the 'true' evolution of the horizontal wind field in response to the various surface forcing factors.

The horizontal pressure gradients were calculated from the wind field to avoid fictitious accelerations as discussed in Chapter 3. The details of these calculations are outlined in the Appendix.

### 4.2.1 Results

Time-mean precipitation maps based on the sub-synoptic network of climatic stations show the average distribution of precipitation in the mesoscale. Cyclonic and purely convective precipitation are expected to be comparatively irregular in their incidence and their effects become smoothed when long periods are considered. On the other hand, surface forcing factors or topographical influences are permanent features. They produce local deviations from the regional average precipitation and their effects stand out on most monthly or longer-period precipitation maps (Douglas and Glaspoole, 1947). Thus, a good estimate of the topographical precipitation of a region may be obtained from long-term climatic records (Reinelt, 1969). The mean (1931-60) precipitation map for the encompassing spring period, March to May, clearly shows that the higher elevations in the Western Plains also have higher precipitation (Longley, 1972).

The mean spring precipitation patterns, therefore, were chosen to verify the present simulation of late spring upslope weather (see Fig. 7). The period which has been referred to as late spring varies somewhat from year to year with respect to the calendar, thus the March to May precipitation map was considered most appropriate for verification purposes.

The topographic precipitation component, i.e., precipitation due to surface forcing factors, for the Western Plains can be estimated if some reference precipitation value can be determined which is devoid of all topographic influences. Figure 8 shows the precipitation component due to surface forcing factors based on the hypothesis that the generally observed 3 inch value of precipitation is entirely due to non-topographic effects. This leaves 10-30 percent of the total precipitation attributable to surface forcing factors in agreement with Reinelt (1969) that topographic precipitation represents about 37 percent of the total for the foothills and more than 13 percent for the rest of the Western Plains. Figures 7 and 8 show precipitation maxima, or excesses due to surface influences, in two northwest-southeast bands. One band lies over the foothills with fingers extending over the Swan and Cypress hills and a second band lies along the Manitoba escarpment which includes the Turtle, Riding and Duck mountains, as well as the Pembina, Porcupine, and Pasquia hills. This second band extends northwestward from the escarpment just southwest of, and paralleling, the edge of the Canadian Shield. The northwest-southeast band structure of the precipitation pattern, as well as the dry pocket immediately west of the Duck Mountains and Riding

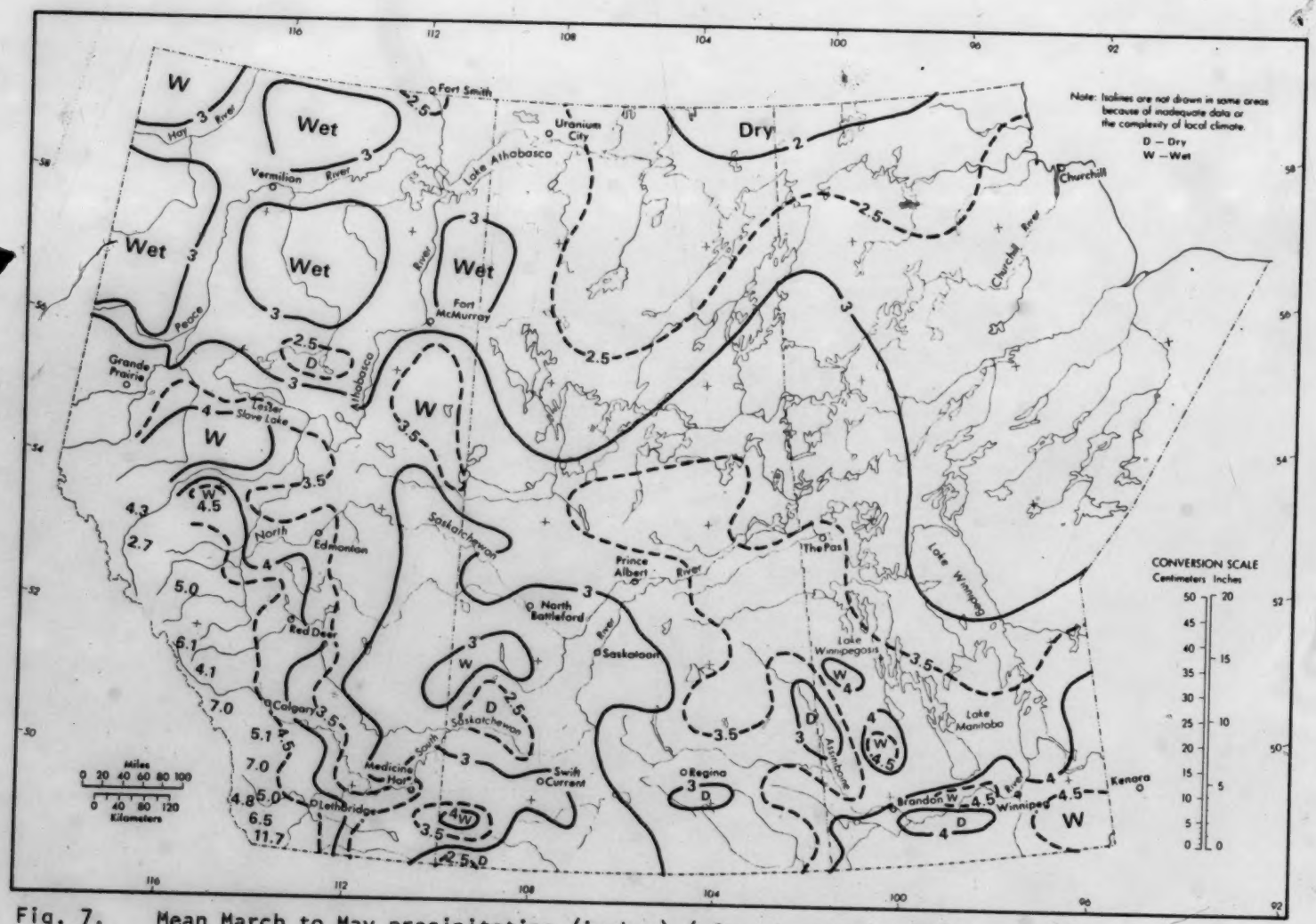


Fig. 7. Mean March to May precipitation (inches) (after Longley, 1972).

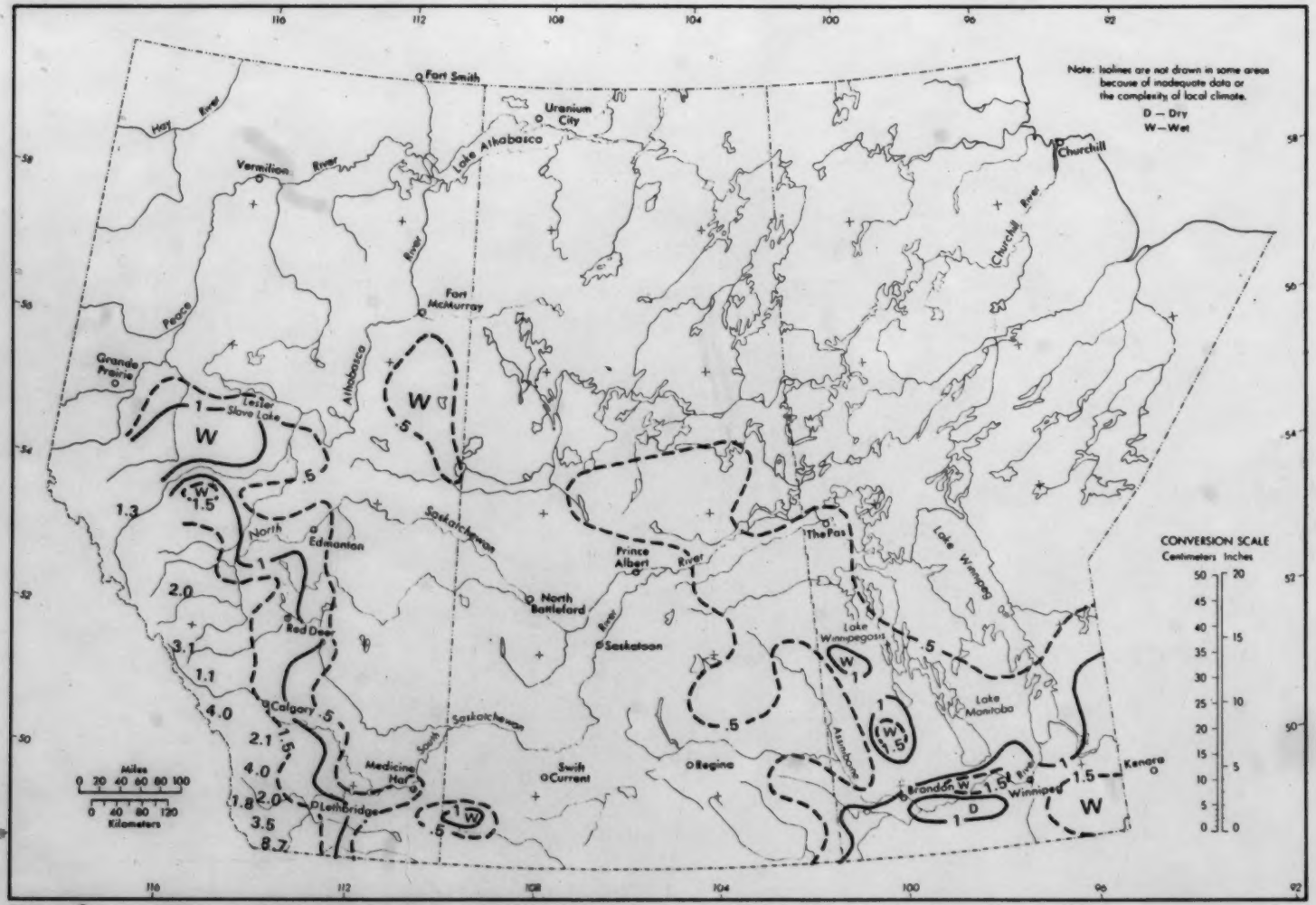


Fig. 8. Mean spring topographic precipitation pattern (inches) (adapted from Longley, 1972).

Mountains, clearly shows the effect of the east-northeasterly circulation of moderately moist arctic air ascending the upland areas of the Western Plains during the spring period.

Figure 9 shows the simulated precipitation pattern produced by the model using 'typical' late spring upslope weather conditions. Although the values of the simulated precipitation rate and the mean topographical precipitation for three months cannot readily be compared quantitatively, it can be seen that the simulated wet and dry patterns correspond quite well with the actual topographic precipitation patterns. A number of factors are believed to contribute to the difference in patterns. These include (a) deviations of actual meteorological conditions from those used to initialize the simulation, (b) the simulation included day-time heating, whereas the mean precipitation pattern includes both day and night precipitation, (c) the lack of mesoscale detail available for the drag and transport coefficient distributions, and (d) evaporation of precipitation below cloud base, and wind transport of droplets have been neglected. It was also realized that the spacing and location of climatic stations lead to inaccuracies in the resultant mean precipitation pattern. Nevertheless, considering the above, the simulated precipitation pattern is remarkably similar to the mean spring topographic precipitation pattern.

Figure 10 shows the vertical velocities $W_h$ generated after six hours of model time. The large-scale relief of the Prairie Provinces may be visualized as a gently-sloping wedge rising from the Hudson Bay lowlands in the northeast to the Rocky Mountains in

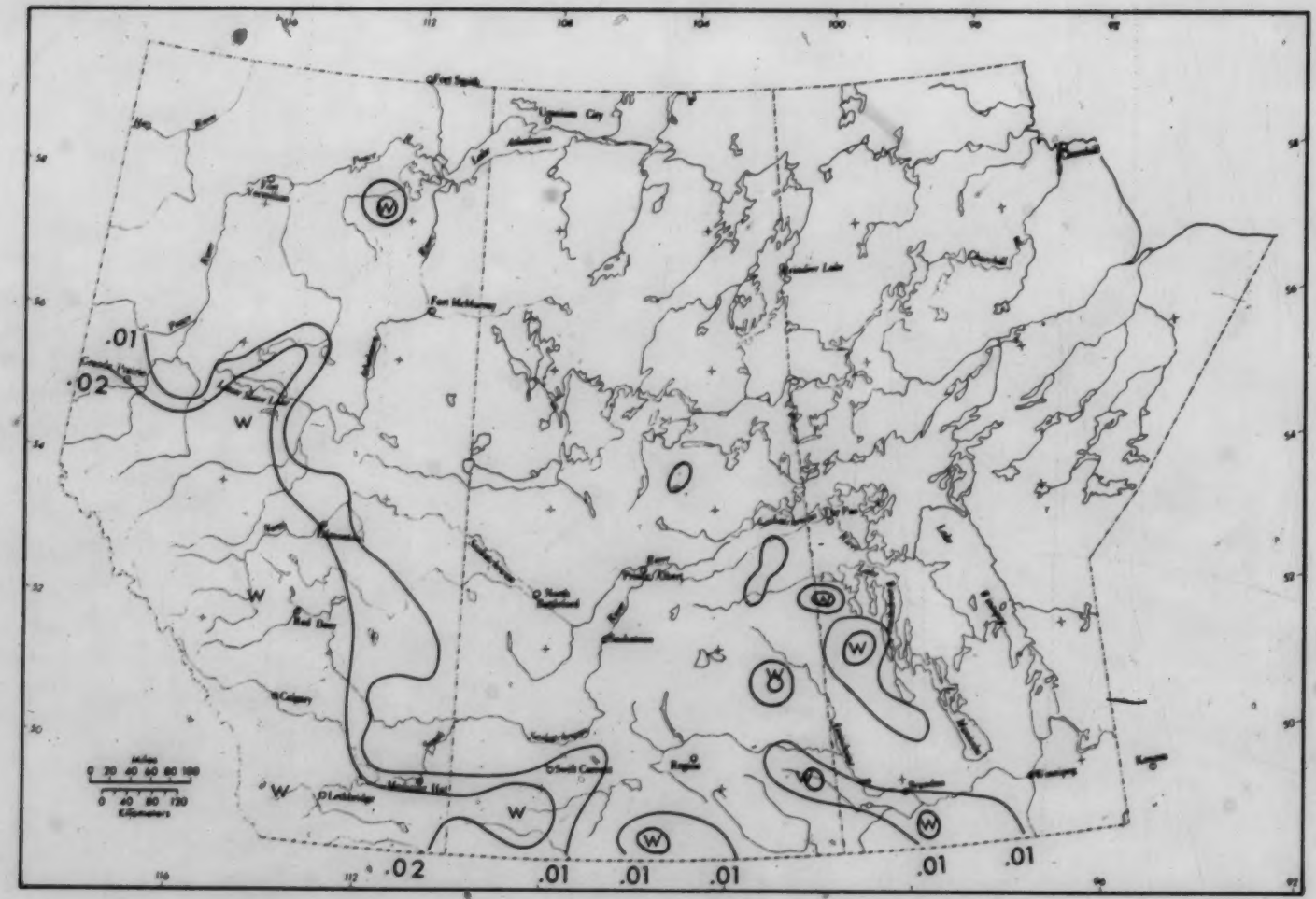


Fig. 9. Simulated topographic precipitation pattern (inches day$^{-1}$).

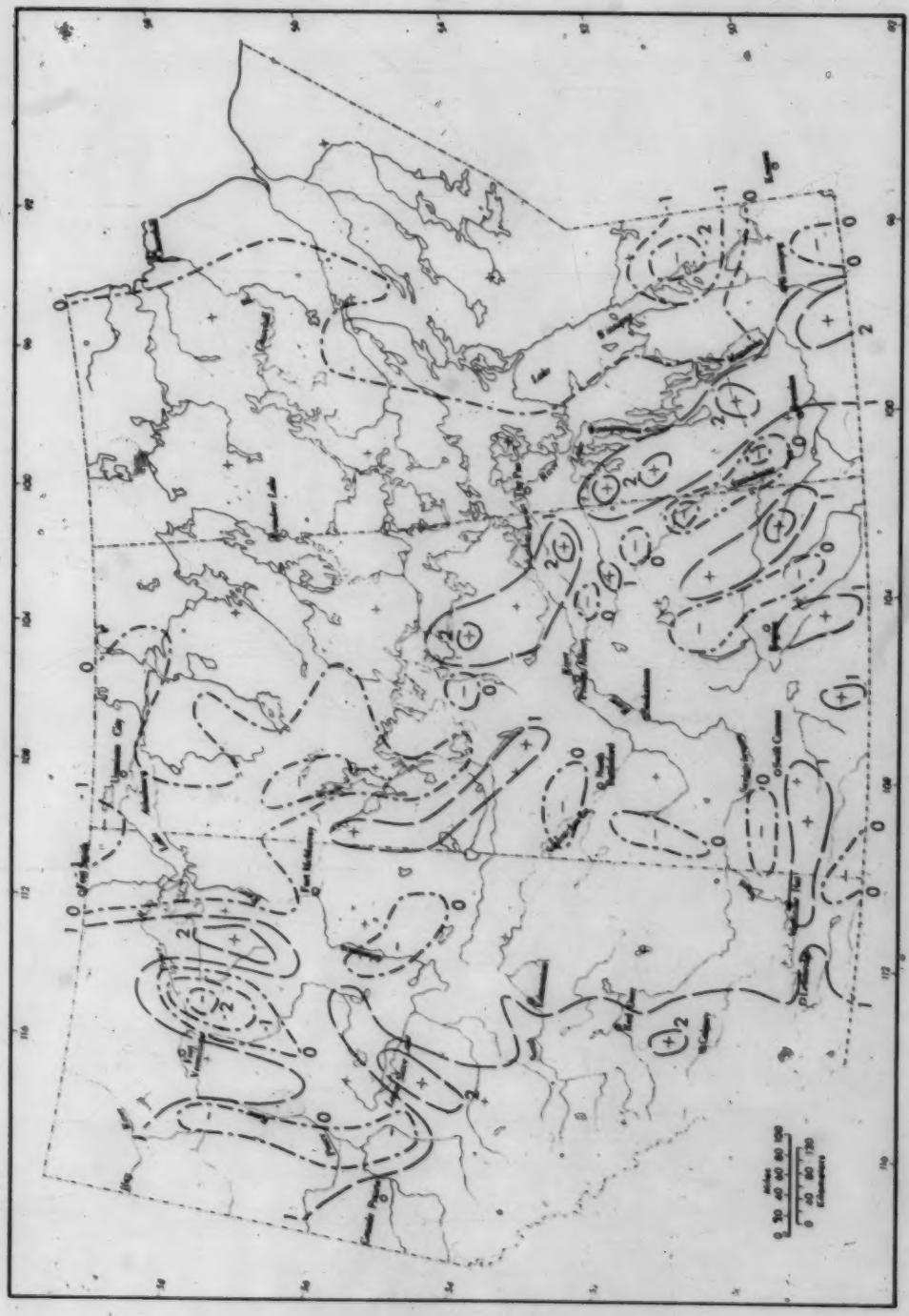

Fig. 10. Simulated vertical velocity pattern (cm $sec^{-1}$).

the west-southwest. An east-northeasterly circulation will, therefore, experience forced ascent and, as a result, small positive vertical velocities are expected over the entire region. Cross isobaric flow leading to horizontal divergence, and the resultant synoptic-scale subsidence will add a negative component to the vertical velocity values as the wind turns more and more out from the high pressure centre in the northeast due to increasing surface roughness from the lowlands to the Rockies.

The simulated vertical velocity pattern in the mesoscale reveals other, generally more significant, features. Looking from east to west in Figure 10, one sees an area of marked subsidence where the Lake of the Woods area drops off to Lake Winnipeg. Further west, there is a north-south band of relatively strong ascent along and northwest of the Manitoba escarpment with maxima immediately upwind of the individual upland areas. Corresponding cellular areas of subsidence or reduced ascent are observed immediately downwind of these upland areas. The extreme vertical velocities in these cells are listed in Table 1. The general area of positive vertical velocities associated with the escarpment can be attributed to the abrupt upslope of the relief. The cellular maxima and minima of vertical velocities associated with the individual upland areas are due to the slowing of the low level flow as it ascends the ridges and a corresponding increase in wind speed immediately downstream from these areas. With the initial wind direction nearly perpendicular to the orientation of the escarpment, significant areas of resultant convergence upstream and divergence downstream from the individual hills produced the

Table 1

Extreme vertical velocities - Manitoba Escarpment

| Upland Area | Max. Upwind $W_h$ | Min. Downwind $W_h$ |
|---|---|---|
| Riding Mountains | +2.1 cm $sec^{-1}$ | -0.9 cm $sec^{-1}$ |
| Duck Mountains | +2.7 cm $sec^{-1}$ | -1.3 cm $sec^{-1}$ |
| Porcupine Hills | +2.3 cm $sec^{-1}$ | -0.8 cm $sec^{-1}$ |
| Pasquia Hills | +2.1 cm $sec^{-1}$ | -0.4 cm $sec^{-1}$ |
| Pembina Hills | +2.4 cm $sec^{-1}$ | -0.9 cm $sec^{-1}$ |
| Wapawekka Hills | +2.9 cm $sec^{-1}$ | -0.5 cm $sec^{-1}$ |

observed maxima and minima in the vertical velocity pattern.

The plains region contains a number of other significant upland areas each of which acts through forced ascent and frictional effects to produce vertical velocities as shown in Table 2. The foothills in the west produced a north-south band of positive vertical velocities with a maximum value of 2.4 cm $sec^{-1}$.

The vertical velocity patterns described above are further complicated by topographic deflection which acts to produce local areas of convergence on the upwind shoulders of the hills and areas of divergence on the downwind shoulders.

Thus, it can be seen that the effects of topographical influences on the mesoscale vertical velocity pattern are far more intricate than just general upslope with the resulting vertical velocity values reduced by synoptic scale subsidence. The general

Table 2

Extreme vertical velocities - other upland areas

| Upland area | Max. Upwind $W_h$ | Min. Downwind $W_h$ |
|---|---|---|
| Moose Mountains | +2.0 cm $sec^{-1}$ | -0.6 cm $sec^{-1}$ |
| Touchwood Hills | +1.5 cm $sec^{-1}$ | -0.5 cm $sec^{-1}$ |
| Dirt Hills | +1.5 cm $sec^{-1}$ | -0.5 cm $sec^{-1}$ |
| Cypress Hills | +1.7 cm $sec^{-1}$ | -0.4 cm $sec^{-1}$ |
| Cheecham Hills | +1.2 cm $sec^{-1}$ | -0.7 cm $sec^{-1}$ |
| Swan Hills | +2.8 cm $sec^{-1}$ | -1.2 cm $sec^{-1}$ |
| Birch Mountains | +3.5 cm $sec^{-1}$ | -2.3 cm $sec^{-1}$ |

upslope motion is complicated by mesoscale frictional convergence and divergence effects associated with the individual upland areas, subsidence resulting from local downslope and the effect of spatial variations of momentum fluxes due to nonuniform surface roughness.

Figure 11 shows the corresponding inversion deformation pattern. It has a marked similarity to the terrain relief with the displacement of the top of the boundary layer or inversion base having maxima generally one grid length upwind from the ridges or upland peaks. Defining the location of an upland area as the position of the appropriate local maximum grid point terrain height value, the inversion deformation was found to vary from 20 to 50 percent of the terrain height as shown in Table 3.

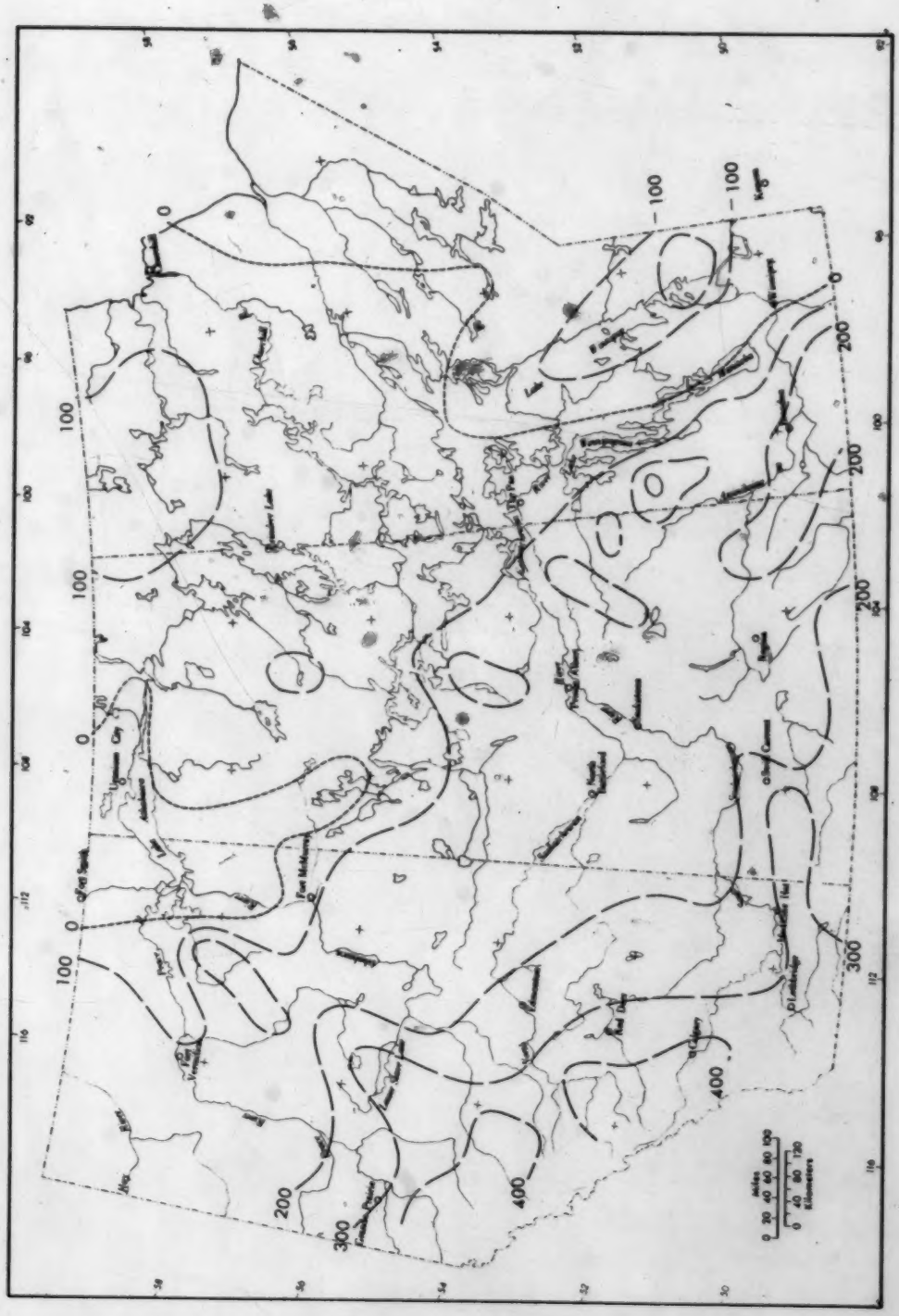


Fig. 11. Simulated inversion deformation pattern (m).

Table 3

Inversion deformations

| Upland area | Terrain Ht. (m) | Inversion Deformation (m) | $\Delta h/Z_o \times 100$ |
|---|---|---|---|
| | $Z_o$ | $\Delta h$ | |
| Foothills* | 983 | 399 | 40.6 |
| Cypress Hills | 1086 | 375 | 34.5 |
| Swan Hills | 1084 | 434 | 40.0 |
| Dirt Hills | 926 | 276 | 29.8 |
| Moose Mountains | 723 | 249 | 34.4 |
| Touchwood Hills | 684 | 248 | 36.3 |
| Birch Mountains | 702 | 259 | 36.9 |
| Cheecham Hills | 691 | 151 | 21.9 |
| Riding Mountains | 632 | 245 | 38.8 |
| Duck Mountains | 639 | 304 | 47.6 |
| Porcupine Hills | 596 | 276 | 46.3 |
| Pasquia Hills | 523 | 237 | 45.3 |
| Waspawekia Hills | 597 | 204 | 34.2 |
| Turtle-Pembina | 589 | 271 | 46.0 |

*The foothills are defined as a test area of 14 grid points west of Red Deer.

Due to the size and detail of the area of interest, a selected cross section, approximately parallel to the flow, was constructed to display graphically the relationship between the terrain relief, vertical velocities, inversion deformation, and limited convective precipitation. This cross section, shown in Figs. 12, 13 and 14, reveals an apparent inconsistency. The vertical velocity associated with the Riding Mountains was larger than that associated with the foothills, yet the inversion deformation and the rate of precipitation was greater in the latter area. This resulted from the much larger transfer coefficients and consequently greater vertical heat fluxes in the foothills region. The increase in the thickness of the mixed layer was due to the last term of equation (30). The increase resulted from the incorporation of air, whose potential temperature was the same as that of the column, in order to prevent the development of a superadiabatic layer at the top of the mixed layer whenever the capping inversion was wiped out by heating from below. This simulates the well-known effect that mountains and their foothills act as effective heat sources which tend to promote precipitation of a convective nature. The subsequent release of latent heat further warms the layer and increases the inversion deformation. Thus, it can be seen that topography contributes significantly both to thermal convection and to forced ascent with frictional effects. However, due to mutual interactions it is usually difficult to separate the relative contributions of the various surface forcing factors to the resultant limited convective showers.

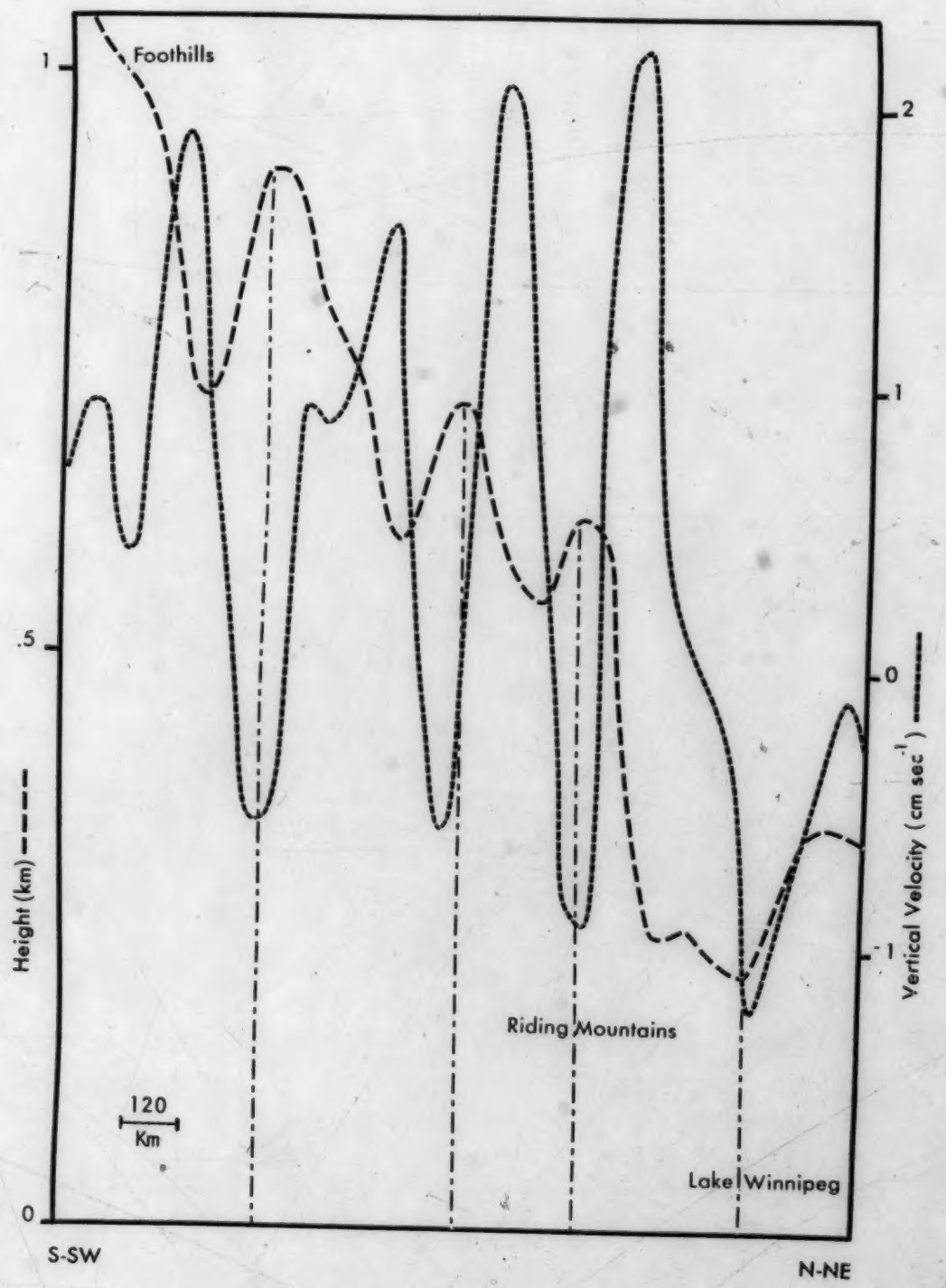


Fig. 12. Vertical velocity - topography cross-section .

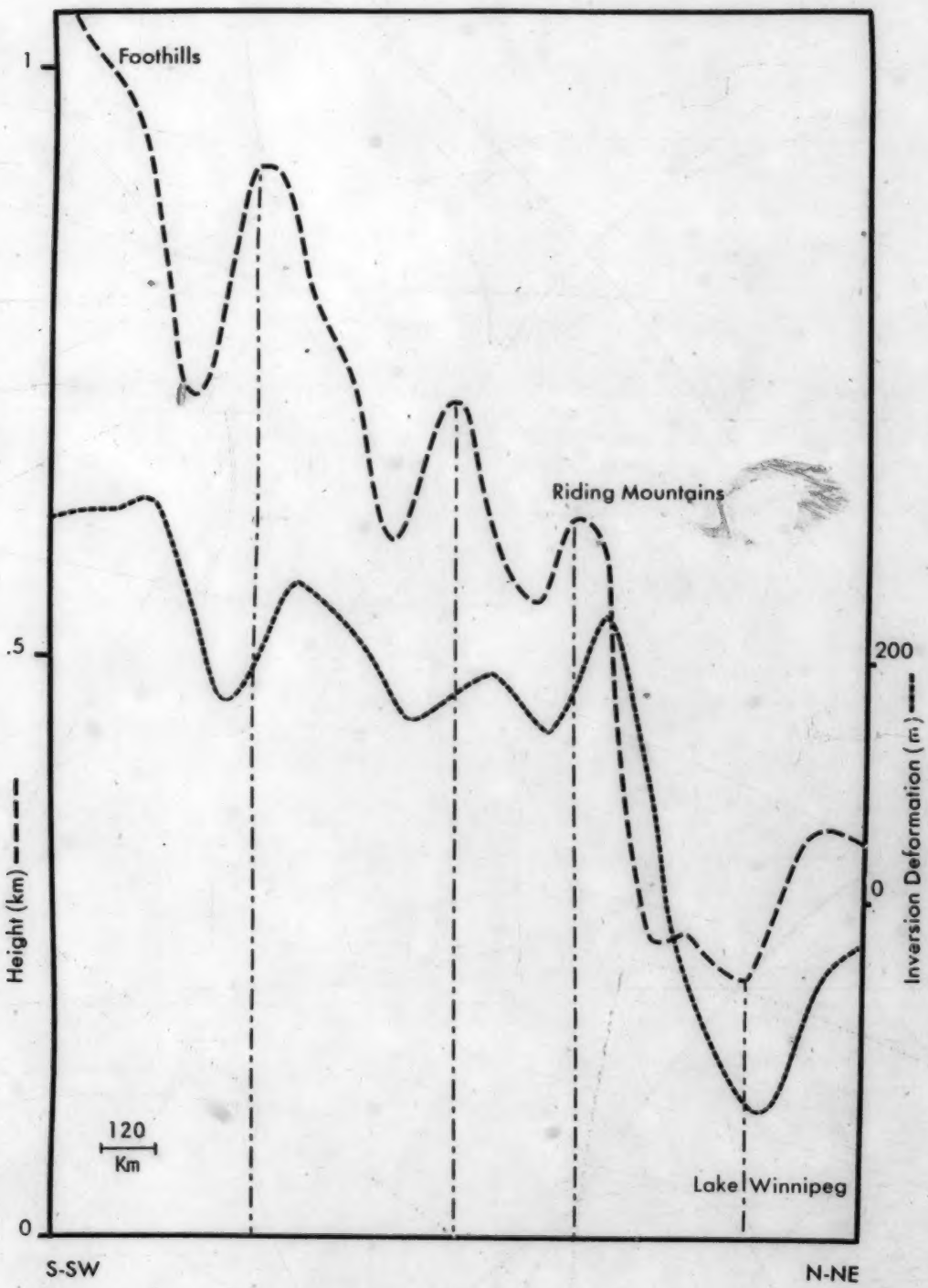


Fig. 13. Inversion deformation - topography cross-section.

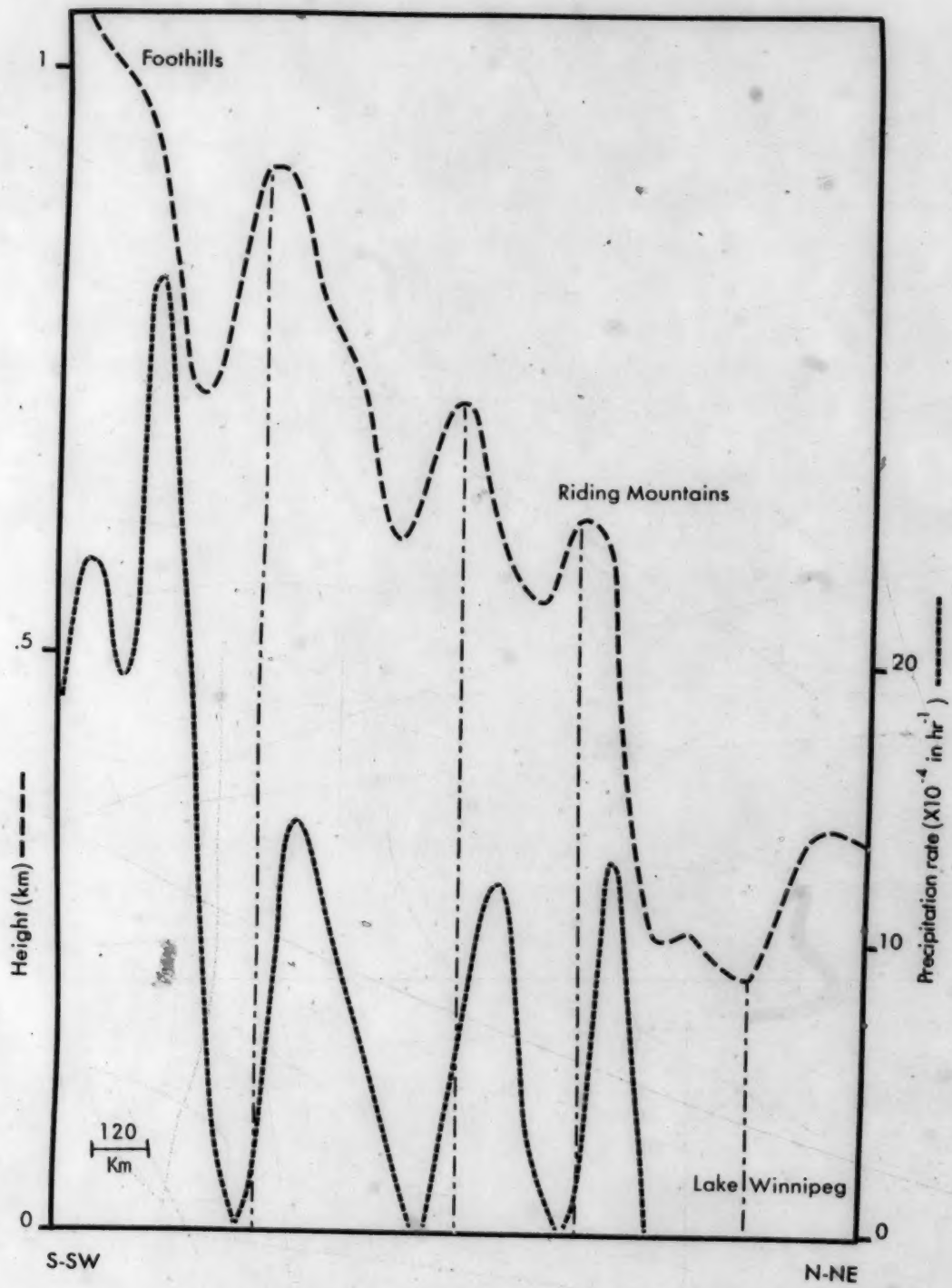


Fig. 14. Precipitation - topography cross-section.

## 4.3 A Sensitivity Experiment

The relative contribution of surface heating compared with the topographical effects of upslope and frictional convergence or divergence to the evolution of mesoscale boundary-layer weather patterns with limited convective precipitation was investigated by running the model while neglecting surface eddy heat fluxes. Meteorological conditions identical to those used in the preceding simulation were used so that the various resultant fields could be compared. The sensitivity run was an attempt to isolate the influence of surface heating and to assign a relative magnitude to it. Although the various surface forcing factors are highly interrelated, some separation was possible.

The experiment involved setting the transfer coefficients for heat equal to zero throughout the integration period. Vertical fluxes of momentum and moisture were not interrupted.

Figure 15 shows the inversion deformation generated after six hours of model time. The most obvious differences between this pattern and the inversion deformation pattern obtained in the simulation of typical late spring upslope weather were the generally much smaller values of the inversion deformation. The relative magnitude of the reduction in the inversion deformation may be illustrated by considering the two equal-size test areas outlined in Figure 15. The removal of vertical eddy heat fluxes resulted approximately in a 35 percent reduction in the inversion deformation over the western area where the transfer coefficients were relatively large and a 10 percent reduction for the eastern area where the transfer coefficients

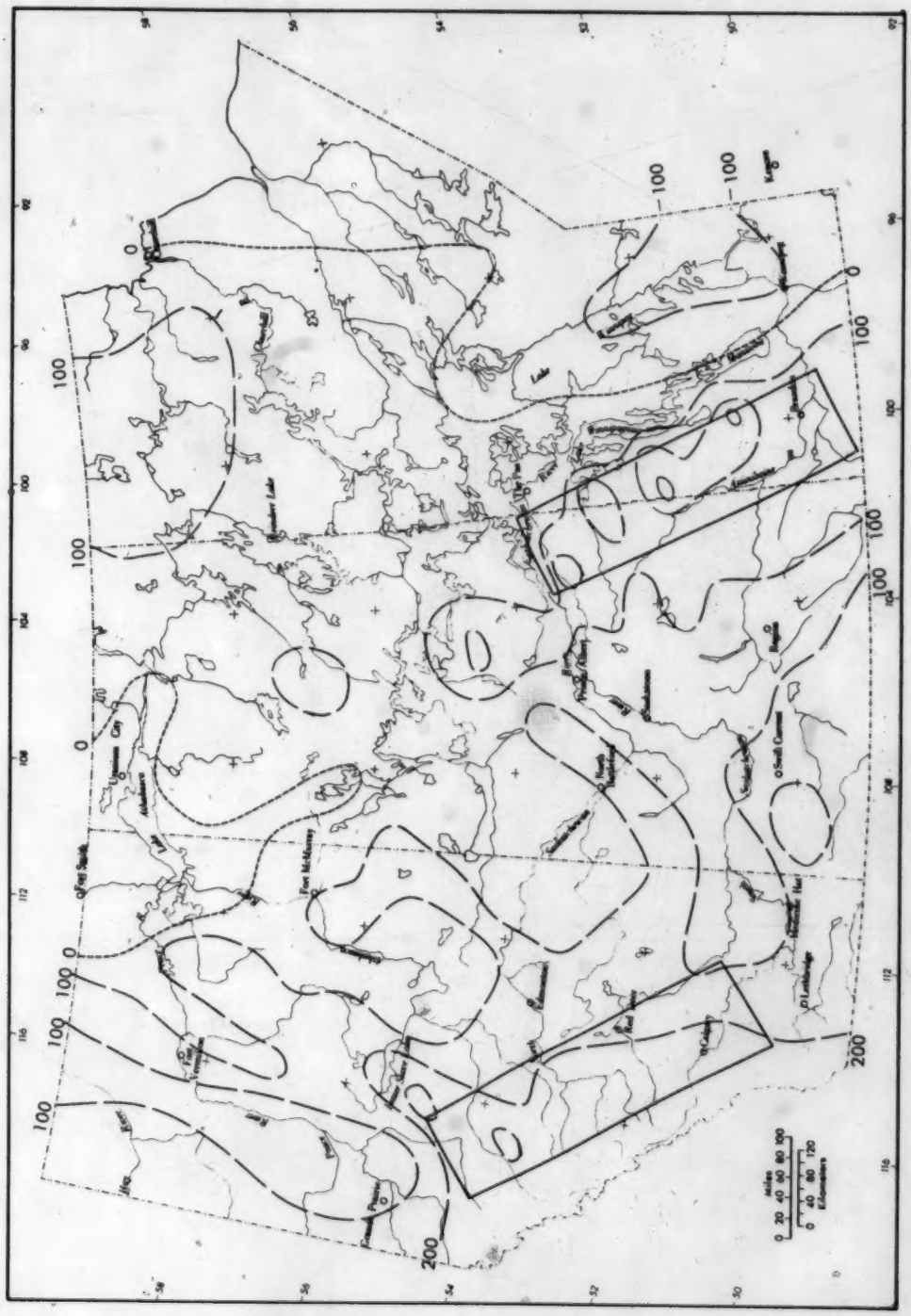

Fig. 15. Simulated inversion deformation pattern, $C_H = 0$.

were smaller in magnitude. This indicates the relative importance of surface heating to the resulting inversion deformation and ultimately to the intensity of the limited convective precipitation. Figure 16 shows the reduced precipitation area that resulted when vertical eddy heat fluxes were neglected. This further illustrates the significance of surface heating. Thus, it was concluded that the area and intensity of limited convective precipitation which occurs when a moderately moist unstable arctic air mass advances upslope over the Western Plains is significantly enhanced by the inclusion of surface heating.

## 4.4 Simulation of an Observed PBL Weather Pattern

The model has been developed through consideration of conditions characteristic of late spring upslope weather on the Canadian Western Plains. The following case study provided an independent test of the ability of the model to simulate boundary-layer weather patterns derived from observations.

In order to reproduce a persistent limited convective precipitation situation maintained by an east-northeasterly circulation of tcA air interacting with the Western Plains, we began by establishing representative air mass and flow parameters for the period and area of interest. This was achieved through an examination of the tephigrams and hodographs for the upper air stations within or near the grid. Representative soundings were then chosen and used to establish the air mass structure specified to be uniform over the entire grid at $t = 0$. A low-level flow pattern was obtained by calculating the vertical mean of the mixed-layer winds for the

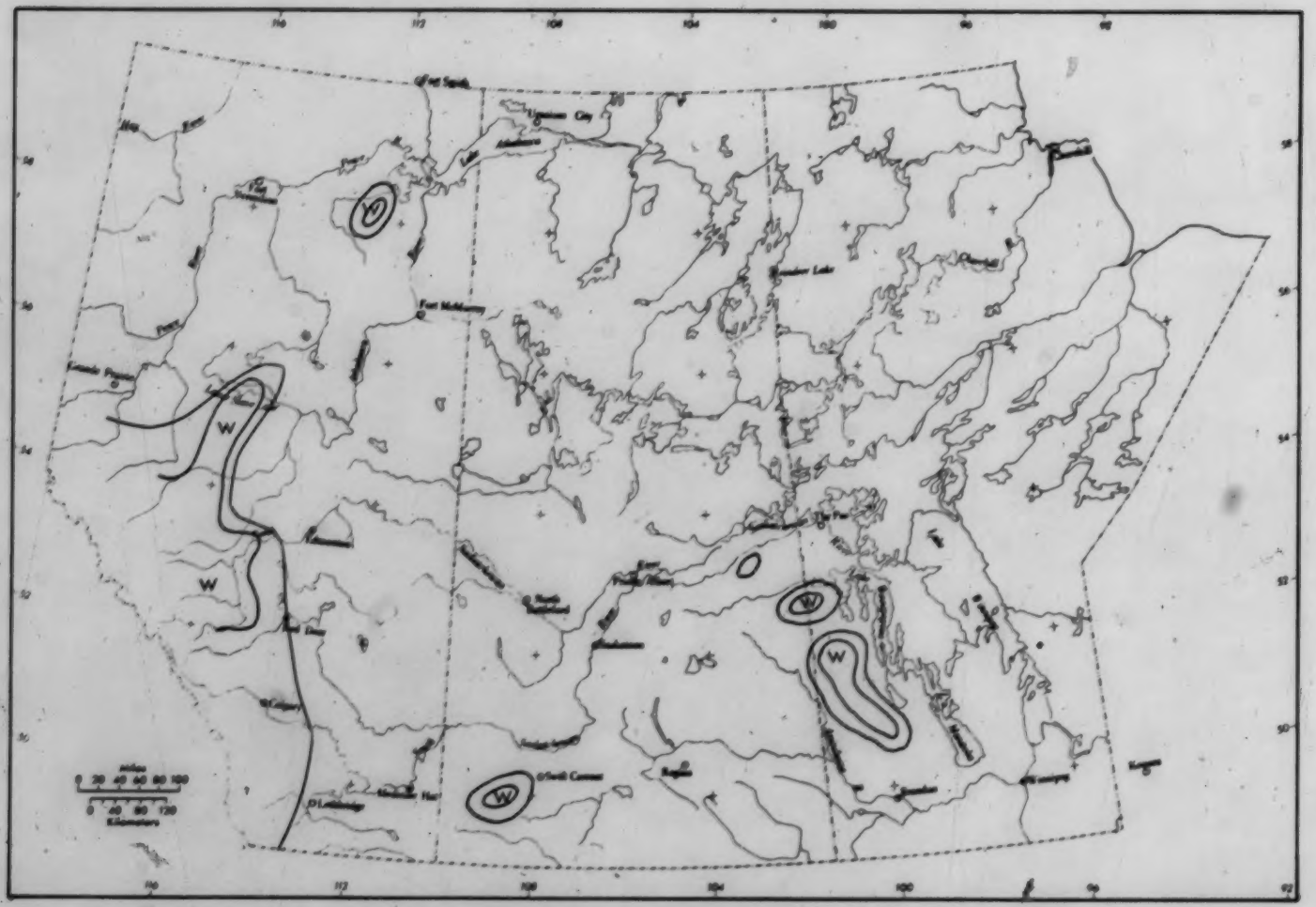

Fig. 16. Simulated precipitation pattern, $C_H = 0$.

representative upper air stations.

4.4.1 Case Study (April 26, 1969)

The synoptic situation of April 26, 1200Z (Figs. 17, 18, 19) has been described by Reinelt (1969) as being representative of shallow upslope circulations east of the Rocky Mountains. The surface map has an Arctic high pressure centre northeast of Great Bear Lake with a ridge line extending southeastward over Hudson Bay. The high, in conjunction with a deep low located in North Dakota, has established a persistent northeasterly flow over most of the Western Plains. A surface trough, which extended northwestward from the low-pressure centre along a line from the Cypress Hills to just east of the Swan Hills, has produced a northwesterly flow over Alberta west of the trough line. The low-level flow was remarkably similar to the mean May surface streamline pattern (Fig. 1). The 700 and 500 mb maps (Figs. 18 and 19) showed a moderate to strong northeasterly circulation of considerable depth in Saskatchewan and Manitoba north of the intense low, but over Alberta the northeasterly flow had become weak to moderate and quite shallow under the ridge that was intensifying at upper levels.

A narrow spur of precipitation paralleling the Rockies was maintained by upslope flow (Reinelt, 1969), and was intensified by low-level convergence along the trough. A second area of precipitation in southern Manitoba and Saskatchewan was, at least partly, of cyclonic origin. The trace of precipitation in northern Manitoba was attributed to weak upslope and to low level convergence due to onshore flow.

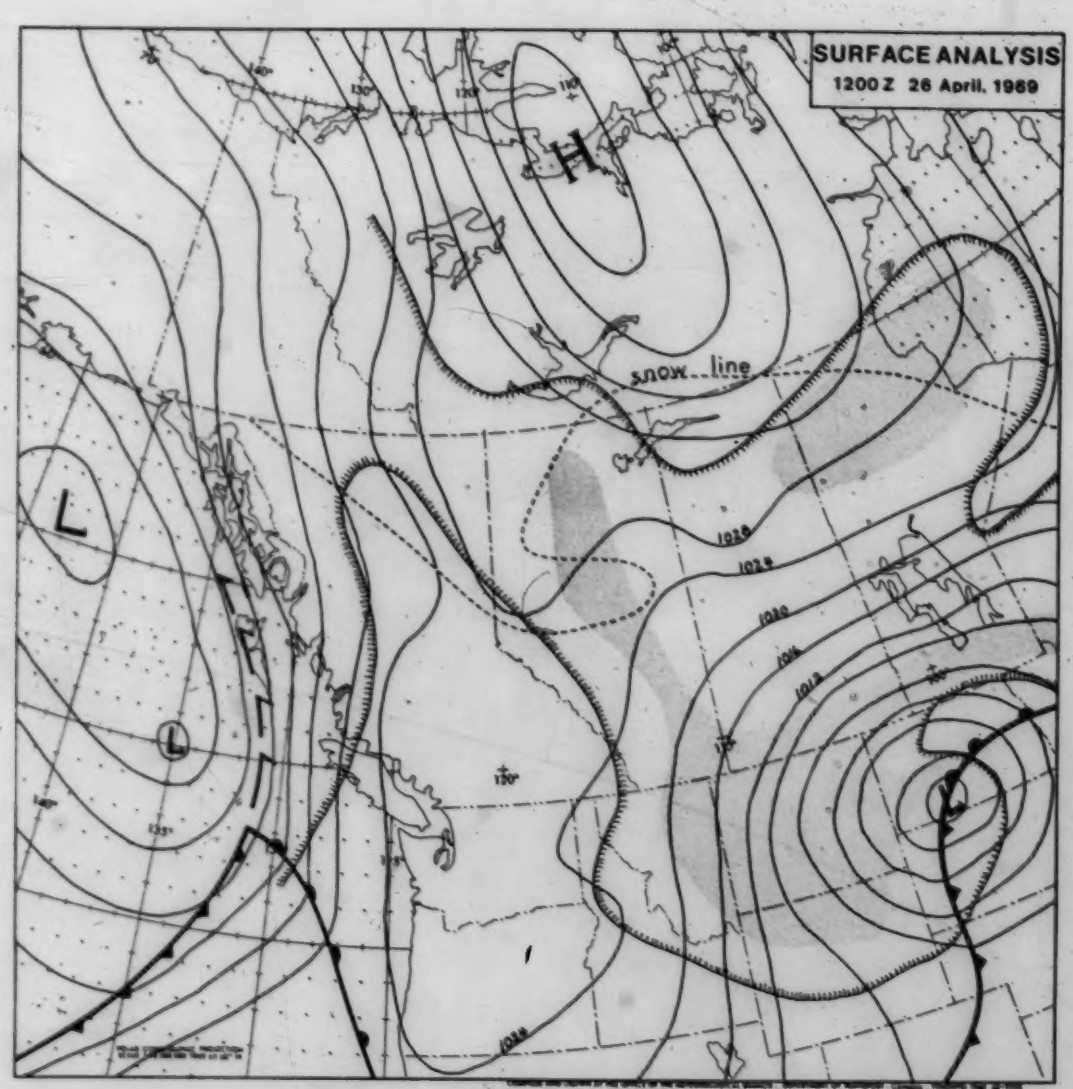


Fig. 17. Surface analysis 261200 GMT, April 1969.

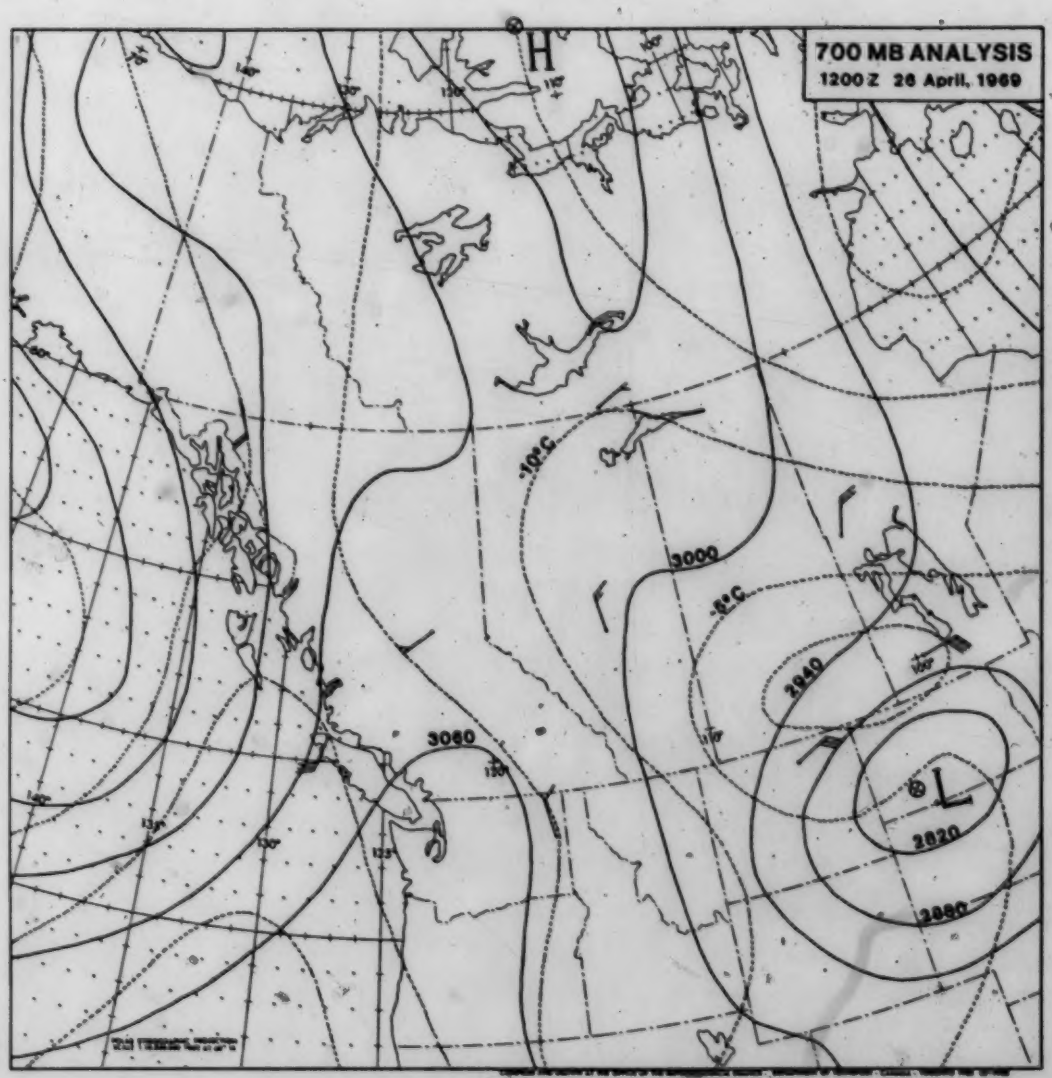


Fig. 18. 700 mb analysis 261200 GMT, April 1969.

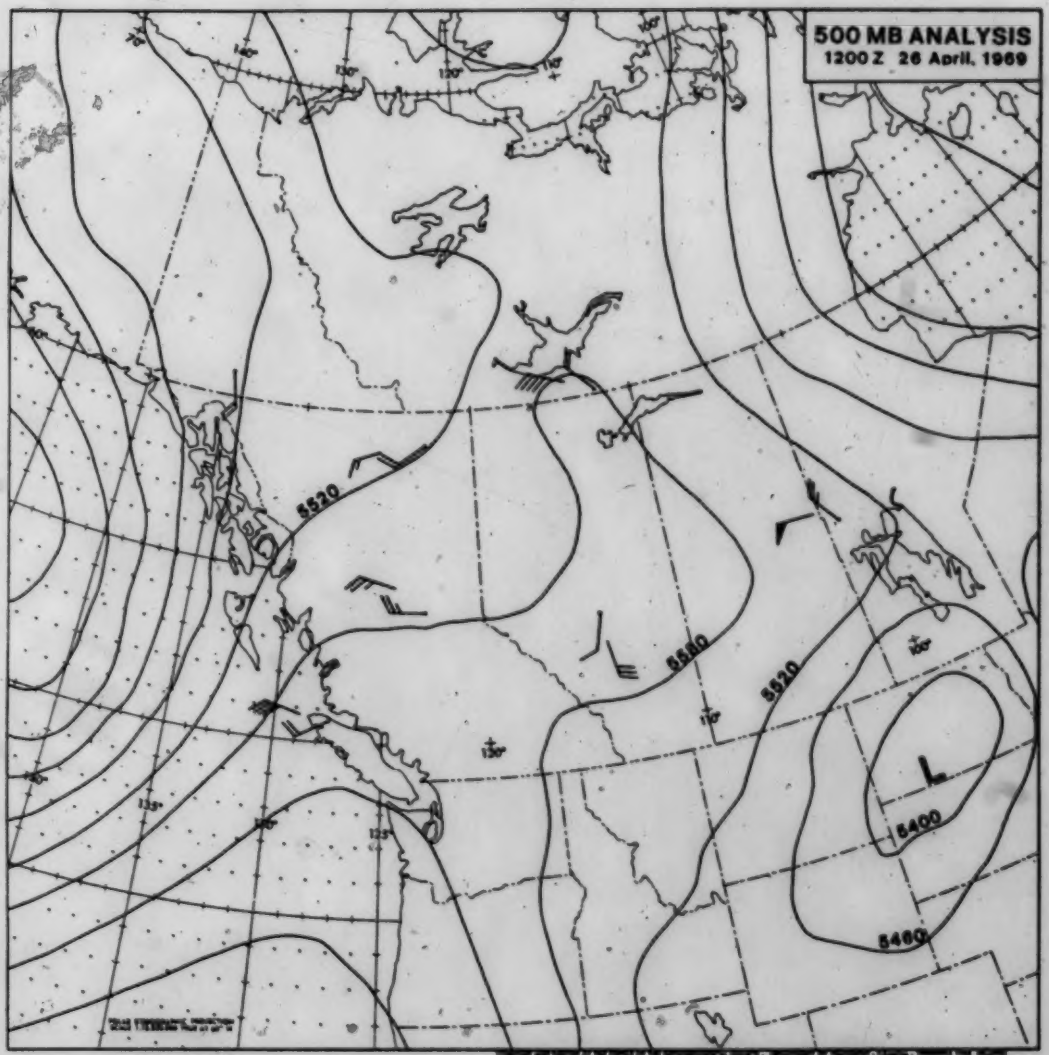


Fig. 19. 500 mb analysis 261200 GMT, April 1969.

An examination of the tephigrams for the upper air stations within or near the grid indicated that the 261200 GMT sounding for The Pas was representative of conditions in the arctic air mass modified to tcA by interacting with the Canadian Shield, but not yet modified by contact with the Western Plains. This was the desired state for initialization of the model. Air mass parameters for the model, therefore, were taken mainly from the 261200 GMT sounding for The Pas. Some adjustments were made based on the 270000 GMT sounding for The Pas and the 261200 GMT and 270000 GMT soundings for Fort Smith, Edmonton and Glasgow in order to obtain the most representative conditions in the tcA air mass. The initial low-level flow east of the trough was obtained by calculating the vertical mean wind from The Pas' 261200 GMT hodograph, using only those levels which were below the inversion. A similar procedure, based mainly on Edmonton's hodographs, gave the representative low-level flow west of the trough. This provided the flow pattern over the area of interest. The initial conditions were: (a) $T_o$ = 0C, (b) $Td_o$ = -6C, (c) h = 1350 m, and (d) V = 050/8 m $sec^{-1}$ east of the trough and 335/8 m $sec^{-1}$ west of the trough, where the trough was simulated by a column three grid points wide over which a linear transition in wind direction from 335 to 050 degrees took place. The snow-line for 261200 GMT is included in Figure 17. The areas covered with snow were assumed to have surface temperatures of 0C as was the Shield in the east and the mountains along the western edge of the grid. The remaining area was assumed to have an excess surface potential temperature of 4K due to a smaller albedo. Narrow transition zones were included as

in the previous simulation. As no clear-cut outflow boundary existed, the dependent variables were held constant at all lateral boundaries.

The upstream and downstream soundings (Figs. 20, 21, 22, 23) for the period of the weather disturbance show the persistence of the air mass structure being considered as well as some of the changes that occurred to the inversion height over time and space. The low-level wind profiles (see Table 4) for the same stations indicated that the assumption of vertical homogeneity in the horizontal wind field was reasonable.

A successful simulation was defined as the reproduction of the precipitation pattern which actually occurred on April 26, 1969. For verification purposes the actual precipitation pattern was obtained from the daily records of the climatic stations within the area of interest (Fig. 24).

### 4.4.2 Results

Due to the nature of this case, only the spur of precipitation paralleling the Rocky Mountains was considered. The location of this precipitation band was further east and the amount of precipitation was greater than would have been expected on the basis of the mean spring precipitation map alone (see Fig. 7). These aspects of the precipitation band, therefore, were attributed to the effects of the low level trough extending northwestward from the North Dakota low. The precipitation was maintained by upslope flow and persisted through April 26, 1969.

Figure 25 shows the precipitation pattern generated after six hours of model time. The simulated trough had the desired effect.

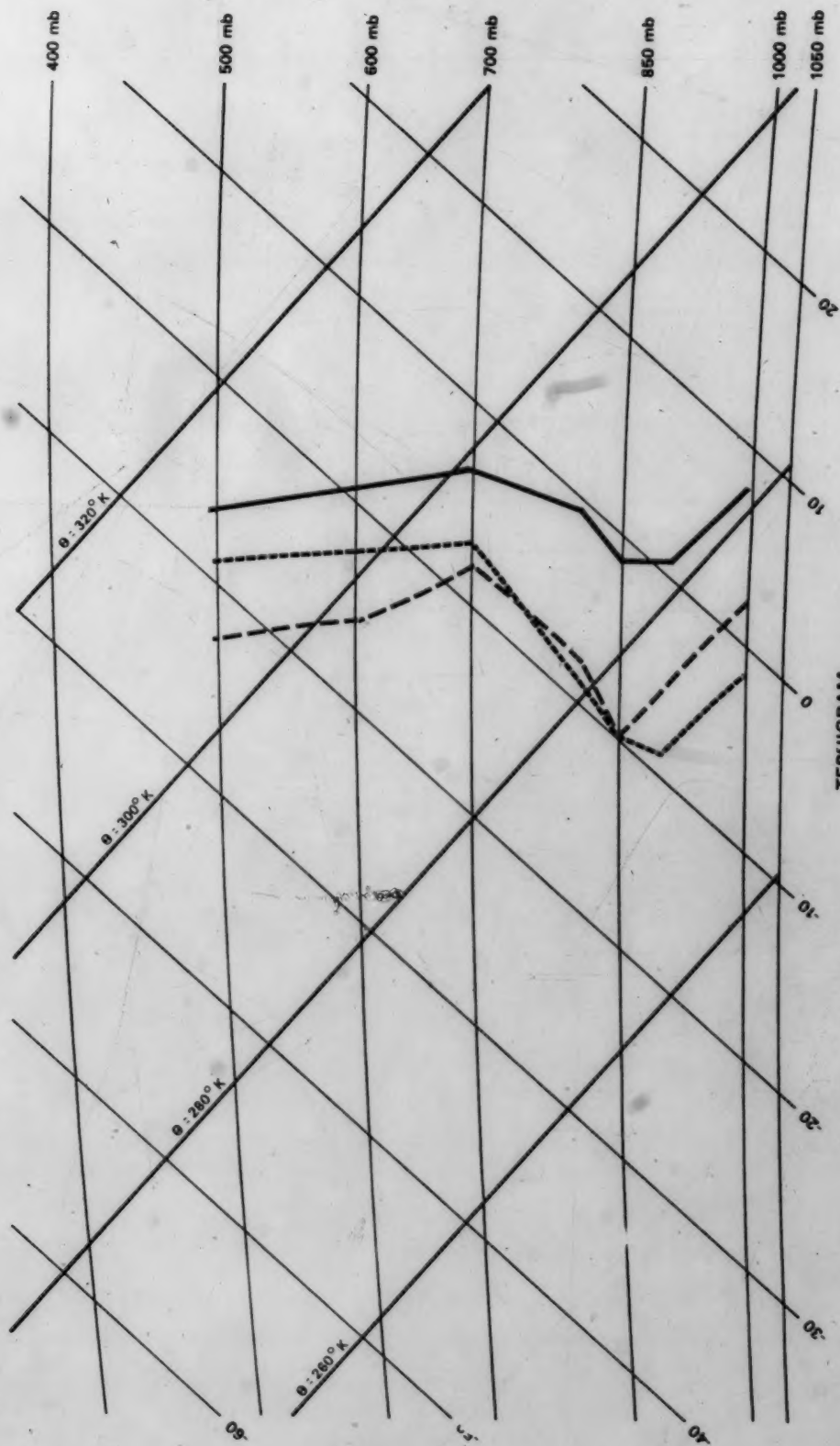


Fig. 20. Tephigrams - The Pas (——261200 GMT, —— 260000 GMT, – – – 270000 GMT).

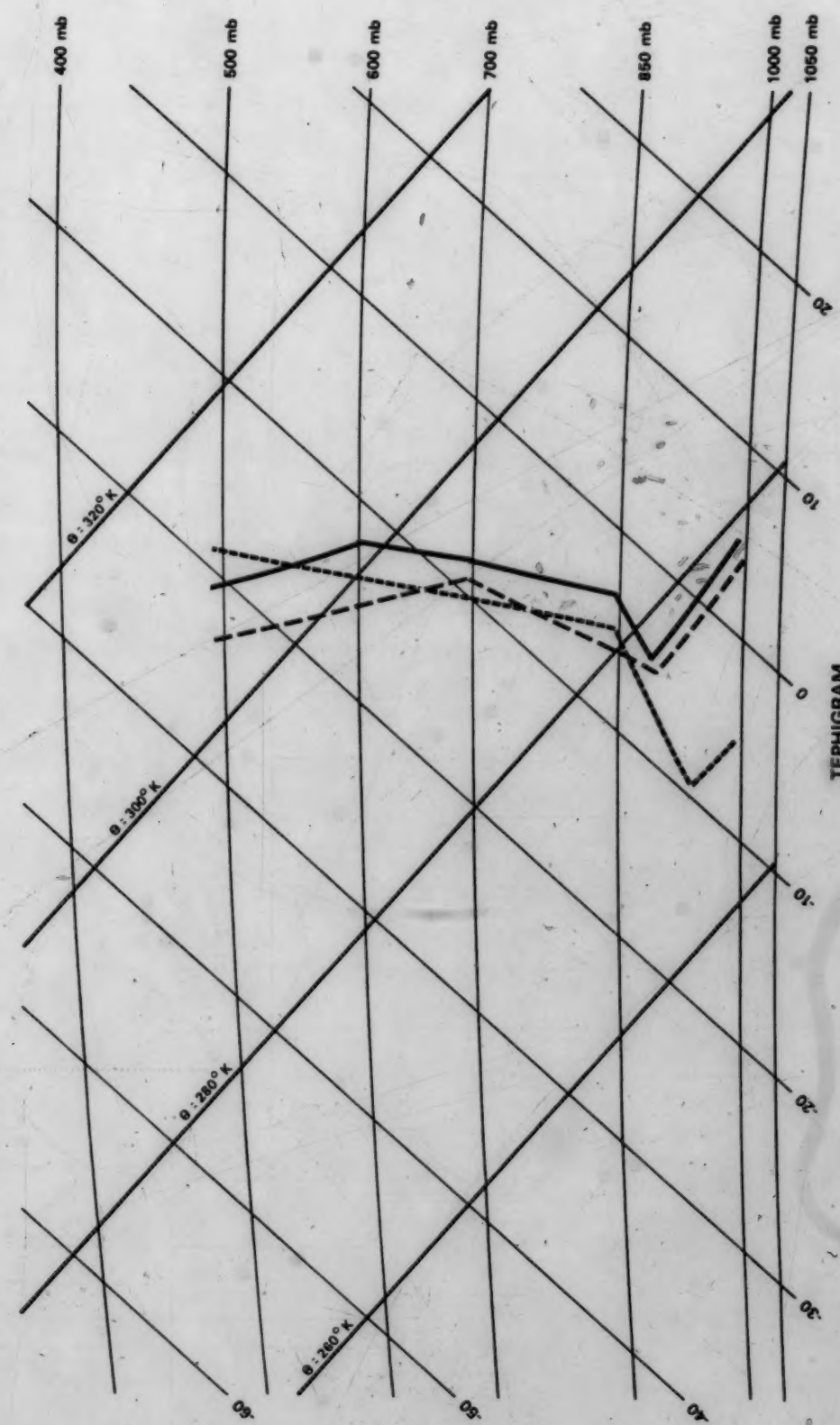


Fig. 21. Tephigrams - Fort Smith (——261200 GMT, —— 260000 GMT, – – – 270000 GMT).

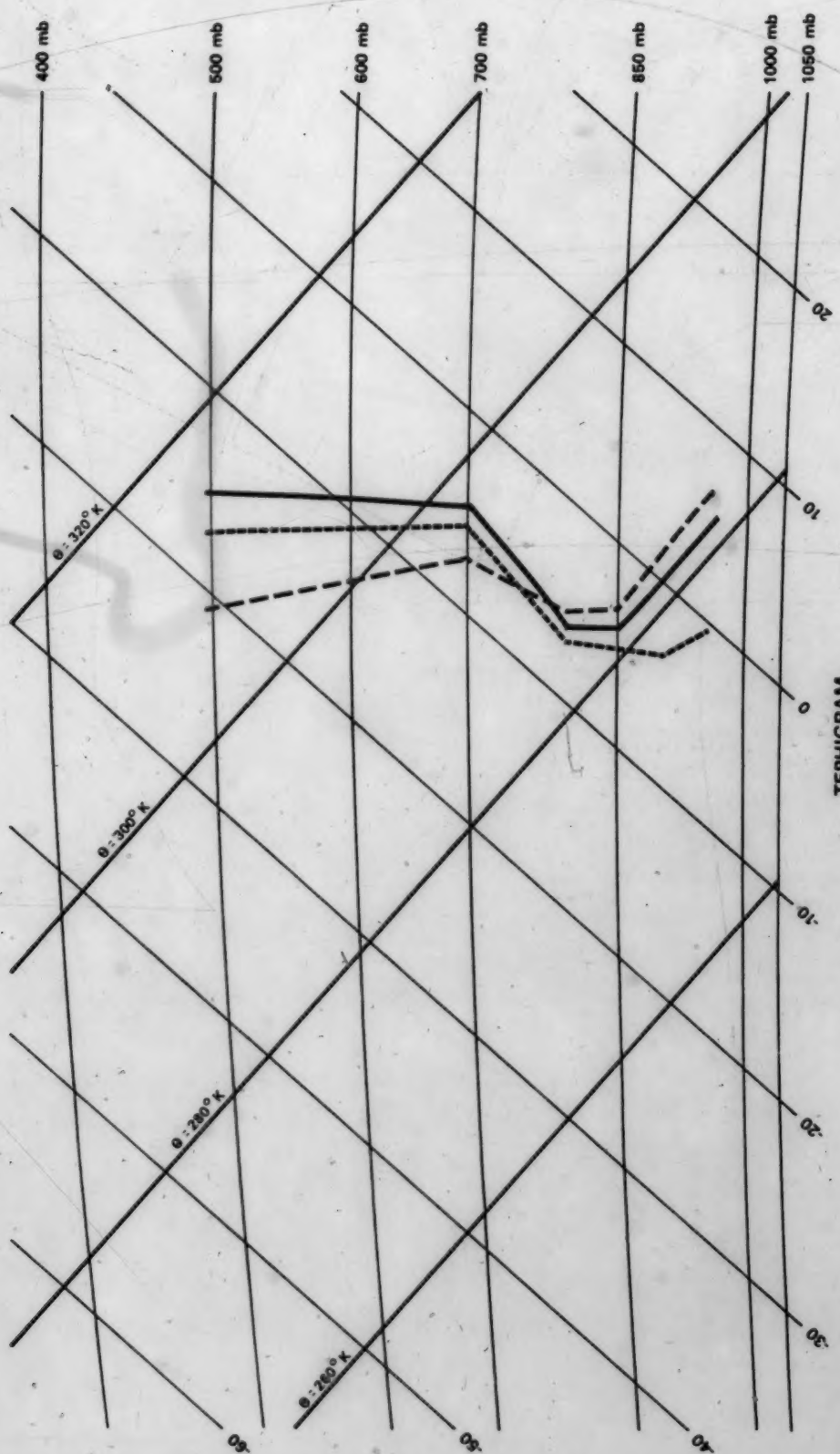


Fig. 22. Tephigrams - Edmonton (—·—261200 GMT, —— 260000 GMT, – – –270000 GMT).

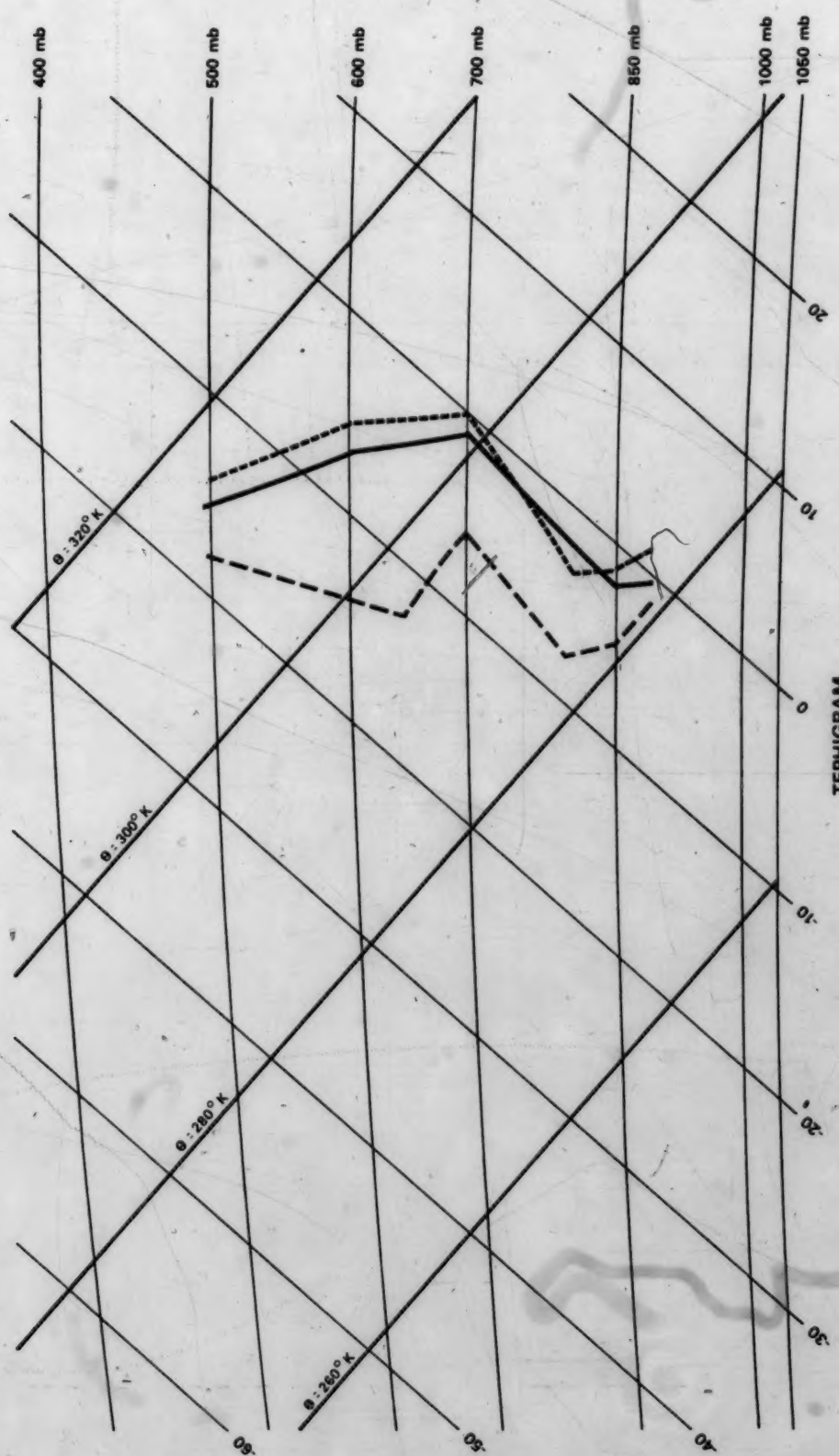


Fig. 23. Tephigrams - Glasgow (—— 261200 GMT, —— 260000 GMT, -- -- 270000 GMT).

Table 4

Low-level Wind Profiles - April 26, 1969

| Station | 261200 GMT | | 270000 GMT | |
|---|---|---|---|---|
| | Height (gpm) | Wind (deg/mps) | Height (gpm) | Wind (deg/mps) |
| The Pas | 273 | 040/08 | 273 | 040/08 |
| | 591 | 050/11 | 621 | 045/08 |
| | 1014 | 054/13 | 1048 | 051/09 |
| | 1456 | 052/10 | 1493 | 056/09 |
| Fort Smith | 203 | 070/04 | 203 | 120/06 |
| | 260 | 070/04 | 245 | 120/06 |
| | 659 | 118/05 | 658 | 121/05 |
| | | | 1085 | 122/05 |
| Glasgow | 885 | 358/14 | 1009 | 018/14 |
| | 1343 | 023/22 | 1461 | 022/16 |
| | 1826 | 054/22 | 1930 | 034/17 |
| Edmonton | 766 | 315/04 | 766 | 338/02 |
| | 1053 | 335/11 | 1061 | 333/03 |
| | 1503 | 337/10 | 1516 | 329/04 |
| | 1978 | 340/10 | 1993 | 326/05 |

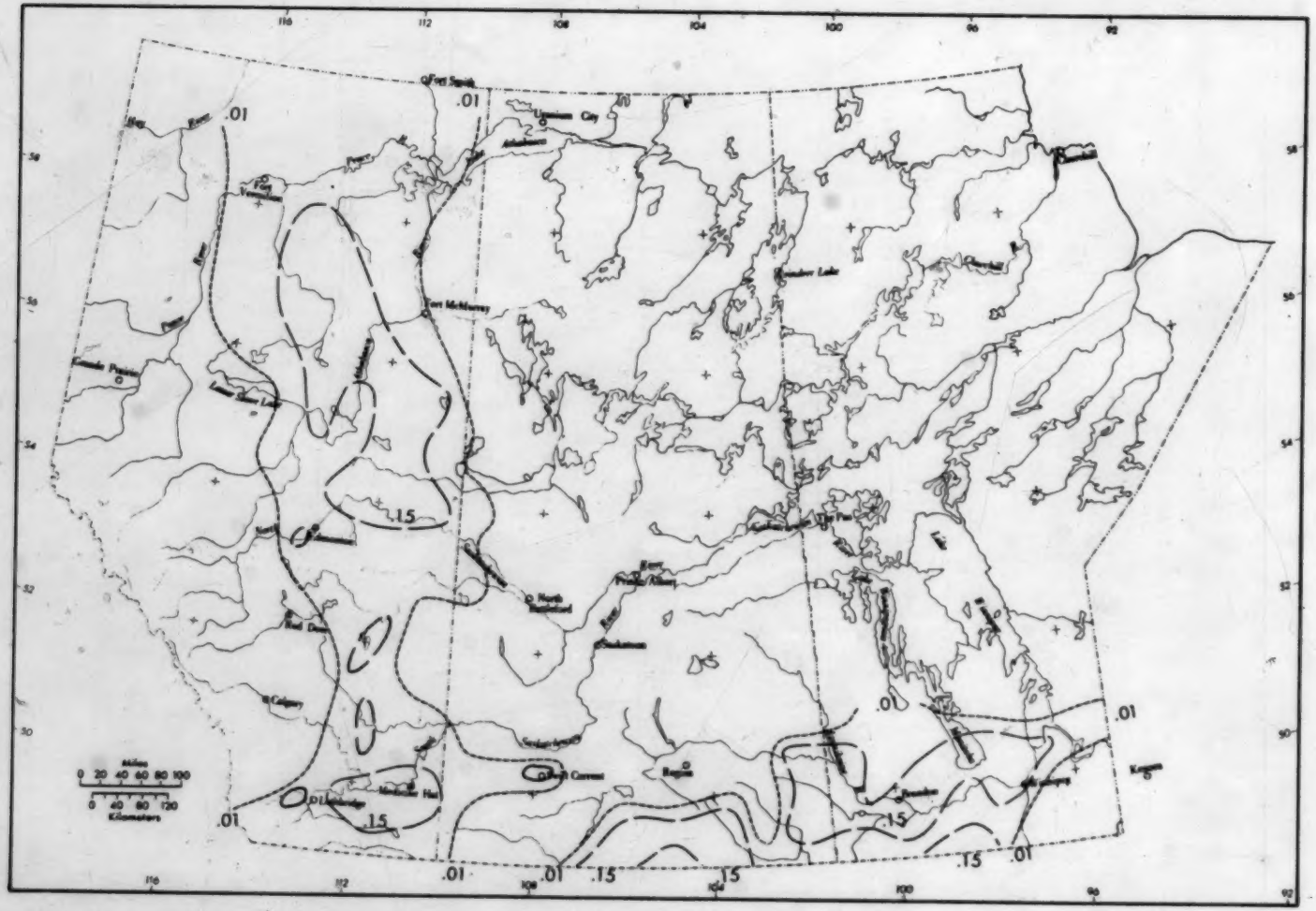


Fig. 24. Precipitation (inches) pattern, April 26, 1969.

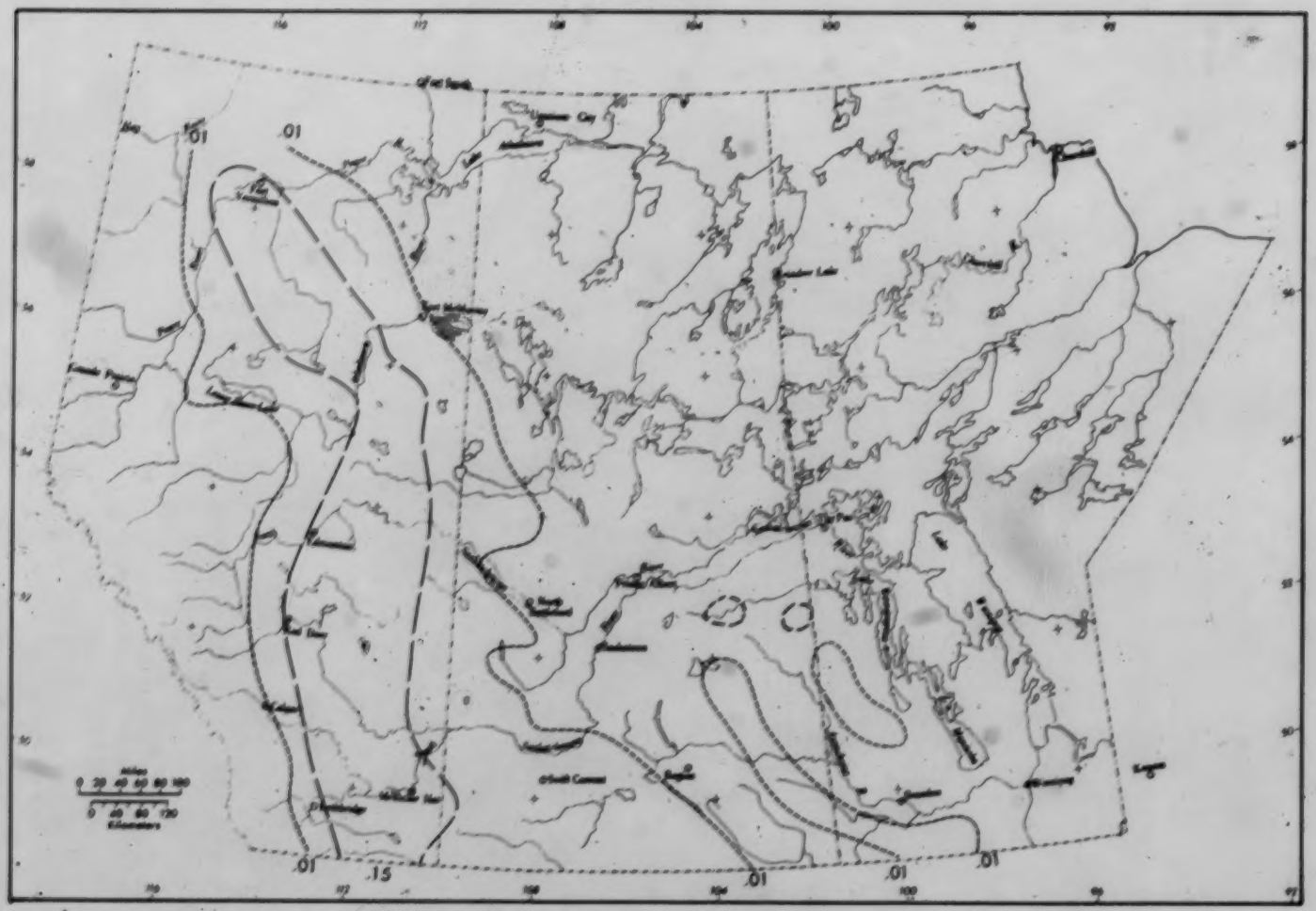


Fig. 25. Simulated precipitation (inches) pattern, April 26, 1969.

The model successfully reproduced the band of precipitation leaving a dry tongue over the foothills, and the amount of the precipitation was enhanced over that produced in the simulation of 'typical' late spring upslope weather. The inclusion of snow cover on the mountains along the western edge of the grid and the subsequent lack of strong upward heat fluxes in this area also contributed to the production of this dry tongue. However, the location and quantity of precipitation was mainly due to upslope flow east of the trough and downslope flow west of the trough.

Figure 26 illustrates the simulated vertical velocity pattern. The most notable feature was the pattern of vertical velocities over Alberta. Here, the vertical velocities were larger than those found in the earlier simulation. This effect was due to strong low-level convergence along the trough and to the slightly stronger low-level flow. Spot value comparisons of the resultant height of the inversion base and mixed-layer winds are given in Table 5. The comparisons, which were severely limited by the number of upper air stations in the area of interest pointed to a successful reproduction of the inversion base height and low-level flow patterns that actually occurred on April 26, 1969, however, the data were too limited to draw any firm conclusions.

Based on the verification of the precipitation pattern and the spot value comparisons of the height of the inversion base and low-level flow pattern it was concluded that the model and the single-layer concept of the PBL could adequately simulate some aspects of an observed boundary-layer weather pattern.

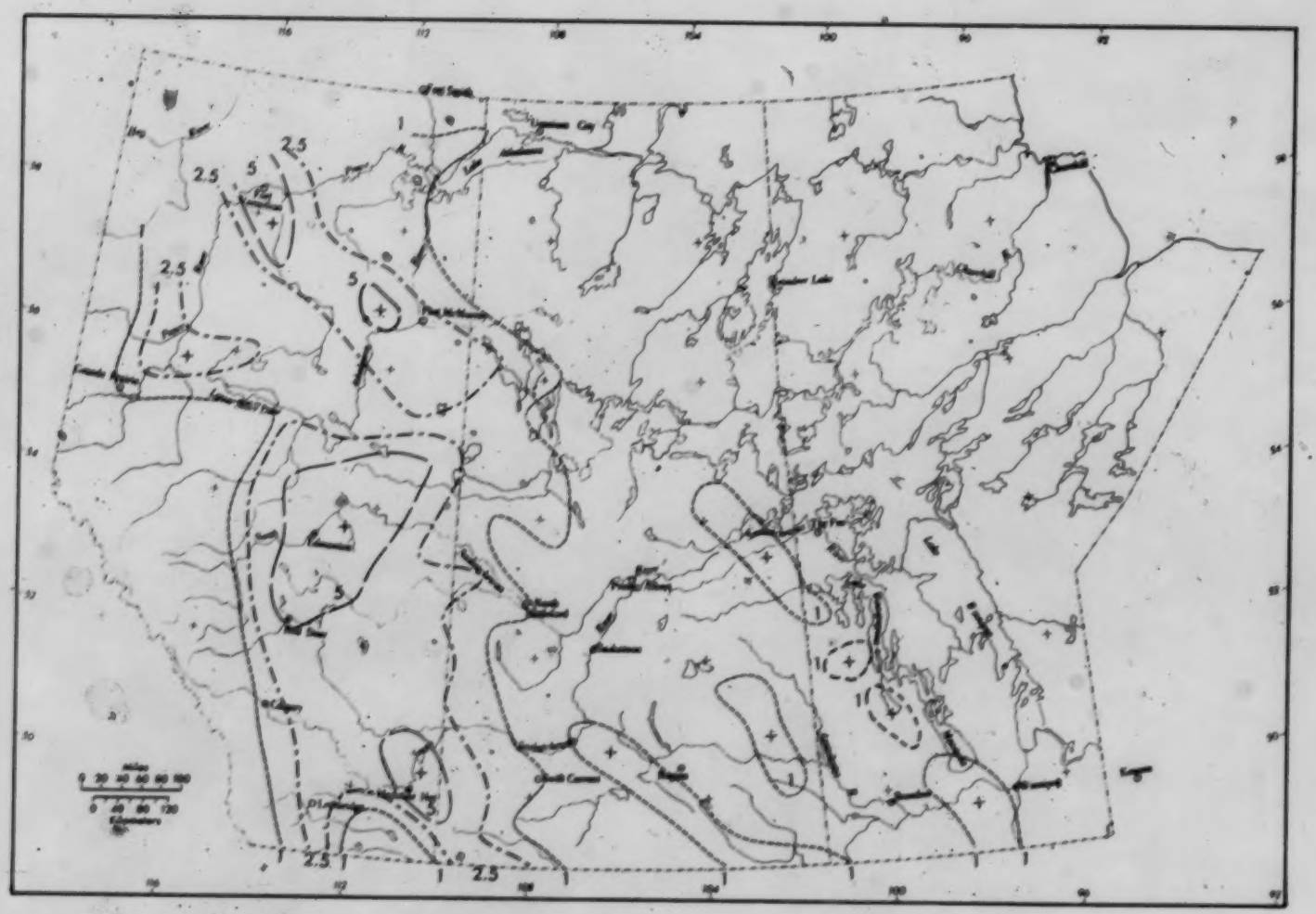


Fig. 26. Simulated vertical velocity (cm $sec^{-1}$) pattern, April 26, 1969.

Table 5

Inversion Base Height and Mixed-layer Winds

| Location | h*(gpm) | h**(m) | Wind***(deg/mps) | Winds**(deg/mps) |
|---|---|---|---|---|
| Edmonton | 1984 | 1965 | 332/06 | 347/05 |
| Glasgow | 1881 | 1713 | 025/18 | 018/06 |
| The Pas | 1475 | 1376 | 049/10 | 049/09 |

*Height of the inversion base at 261200 GMT plus the height of the inversion base at 270000 GMT divided by two.

**Two grid point average in the vicinity of the upper air station.

***Vertical mean of the low-level winds at 261200 GMT plus the vertical mean of the low-level winds at 270000 GMT divided by two.

# CHAPTER 5

## SUMMARY AND CONCLUSIONS

A three-layer mesoscale numerical model has been used to simulate boundary layer weather patterns including limited convective precipitation induced by a moderately moist east-northeasterly circulation of arctic air over the relatively warm, sloping Canadian Western Plains during late spring. Time-dependent calculations were limited to a single 'mixed' layer by parameterizing the interactions of this layer with both the underlying and overlying layers. Limited convective precipitation and the release of latent heat within the layer have also been parameterized. A 47.6 km by 47.6 km grid mesh of 1369 points covering the Canadian Prairie Provinces was used to represent the variables in the mesoscale. The governing equations were solved numerically with surface forcing factors allowed to perturb the 'mixed' layer from its initial conditions until resultant mesoscale boundary layer weather patterns evolved.

Experiments using conditions 'typical' of late spring upslope weather revealed that:

(1) the model atmosphere provided a reasonable representation of the atmospheric structure associated with arctic outbreaks .

over the Canadian Western Plains during late spring.

(2) the mean spring topographic precipitation pattern could be reproduced by the simulated late spring upslope flow with limited convective precipitation. The 'mixed' layer representation of the planetary boundary-layer allowed this to be done relatively simply and with modest computer requirements. Approximately 6.5 minutes of Central Processing Unit (CPU) time and 820 page-minutes of CPU storage on an IBM-360 computer were required to simulate 6 hours of model time.

(3) the limited convective precipitation produced by an east-northeasterly circulation over the Western Plains was intimately related to the configuration of the relief and that upslope weather conditions persisted as long as the low-level flow remained essentially unchanged.

(4) late spring upslope weather is a contributing factor to the upward swing in precipitation amounts over the Western Plains during the spring period.

(5) mesoscale PBL weather patterns exert a dominant control over the location and intensity of perturbations in the spring precipitation pattern.

The sensitivity of late spring upslope weather on the Canadian Western Plains to surface heating has been explored. It was found that the area and intensity of limited convective precipitation was significantly reduced when upward heat fluxes were neglected.

A simulation based on observed initial conditions showed that:

(1) the model was capable of reproducing a limited convective precipitation pattern maintained by upslope flow.

(2) a low-level trough exerts a marked influence on the location and intensity of the precipitation.

This numerical experiment has provided a preliminary look at late spring upslope weather on the Canadian Western Plains. However, a number of problem areas remain. Parameterization, initialization, and verification could all be improved by the incorporation of information on a smaller scale. The lack of detail available for the mesoscale distributions of drag and transfer coefficients is a particularly acute problem. Many more studies are needed to complete our understanding of late spring upslope weather. Nevertheless, it is hoped that a better understanding of this significant weather phenomenon has been achieved. More generally it is hoped that this simulation has provided further insight into mesoscale planetary boundary-layer weather patterns induced by surface forcing factors.

## BIBLIOGRAPHY


Asselin, R.A., 1966: A technique for designing smoothing operators. Department of Transport, Meteorological Branch, CIR-4417, TEC-615, 30 pp.

Ball, F.K., 1960: Control of inversion height by surface heating. Quart. J. Roy. Meteor. Soc., 86, pp. 483-494.

Barry, P.J., 1966: The wind profile. National Meteorology Congress, Roy. Meteor. Soc., June 8-10.

Bergeron, T., 1949: II The coastal orographic maxima of precipitation in autumn. Tellus, 1, pp. 15-32.

Berry, F.A., Owens, G.V., and Wilson, H.P., 1952: Arctic weather maps. United States Navy, Bureau of Aeronautics, Project TED-UNL-MA-501, Applied Research, Operational Weather Analysis.

Bhumralkar, C.M., 1974: Effects of moisture on hydrostatic pressure. J. Appl. Meteor., 13, pp. 174-175.

_____, 1974: Relation between air-sea exchange over the Arabian Sea and the fluctuations of the Western Indian summer monsoon. Rand Paper Series.

Bryson, R.A., 1966: Air masses, streamlines, and the Boreal Forest. Geographical Bulletin, 8, pp. 228-269.

Charette, C.O., 1971: Streamline patterns and terrain-induced vertical velocities in the Canadian Cordillera. M.Sc. Thesis, Univ. of Alberta, 117 pp.

Clark, R.H., 1970: Recommended methods for the treatment of the boundary layers in numerical models. Australian Meteor. Magazine, 18, pp. 51-73.

Cressman, G.P., 1960: Improved terrain effects in barotropic forecasts. Mon. Wea. Rev., 88, pp. 327-342.

Danard, M.B., and Rao, G.V., 1972: Numerical study of the effects of the Great Lakes on a winter cyclone. Mon. Wea. Rev., 100, pp. 374-382.

Deacon, E.L., and Webb, E.K., 1962: Small-scale interactions. The Sea, New York, Interscience, pp. 43-87.

Deardorff, J.W., 1968: Dependence of air-sea transfer coefficients on bulk stability. J. Geophysical Research, 73, pp. 2549-2557.

_____, 1972: Parameterization of the planetary boundary layer for use in general circulation models. Mon. Wea. Rev., 100, pp. 93-106.

Dickison, R.B.B., 1968: The effect of minor relief on the distribution of precipitation. Department of Transport, Meteorological Branch, TEC-700, 16 pp.

Douglas, C.K.M., and Glasspoole, J., 1947: Meteorological conditions in heavy orographic rainfall. Quart. J. Roy. Meteor. Soc., 74, pp. 11-42.

Estoque, M.A., 1961: A theoretical investigation of the sea breeze. Quart. J. Roy. Meteor. Soc., 87, pp. 136-146.

_____, 1962: The sea breeze as a function of the prevailing synoptic situation. J. Atmospheric Sci., 19, pp. 244-250.

Fjørtoft, R., 1955: On the use of space smoothing in physical weather forecasting. Tellus, 7, pp. 462-480.

Gerrity, Jr., J.P., 1967: A physical-numerical model for the prediction of synoptic scale low cloudiness. Mon. Wea. Rev., 95, pp. 261-282.

Haltiner, G.J., 1971: Numerical weather prediction. John Wiley and Sons, Inc., N.Y. and Toronto, 317 pp.

Jones, D.M.A., Huff, F.A., and Changnon, Jr., S.A., 1974: Causes for precipitation increases in the hills of Southern Illinois. Department of Registration and Education, State of Illinois, Report of Investigation 75.

Klein, W.H., 1957: Principal tracks and mean frequencies of cyclones and anticyclones in the Northern Hemisphere. United States Weather Bureau Research Paper, No. 40, 60 pp.

Kurchara, Y., 1965: On the use of implicit and iterative methods for the time integration of the wave equation. Mon. Wea. Rev., 93, pp. 33-46.

Lavoie, R.L., 1972: A mesoscale numerical model of lake-effect storms. J. Atmospheric Sci., 29, pp. 1025-1040.

_____, 1974: A numerical model of trade wind weather on Oahu. Mon. Wea. Rev., 102, pp. 630-637.

Longley, R.W., 1972: The climate of the Prairie Provinces. Climatological Studies, No. 13, Atmospheric Environment, Environment Canada, Toronto, 77 pp.

Mason, B.J., and Howorth, B.P., 1952: The production of rain and drizzle by coalescence in stratiform clouds. Quart. J. Roy. Meteor. Soc., 78, pp. 289-312.

McKay, G.A., and Thompson, H.A., 1968: Snowcover in the Prairie Provinces of Canada. Transactions of the American Society of Agricultural Engineers, Vol. 11, No. 66, pp. 812-815.

Molenkamp, C.R., 1968: Accuracy of finite-difference methods applied to the advection equation. J. Appl. Meteor., 7, pp. 160-167.

Monin, A.S., and Obukhov, A.M., 1954: Basic laws of turbulent mixing in the ground layer of the atmosphere. Akademiia Nauk SSSR, Leningrad, Geofizicheskii Institut, Trudy, No. 24(151), pp. 163-187.

Normand, C.W.B., 1938: On the instability from water vapour. Quart. J. Roy. Meteor. Soc., 64, pp. 47-66.

Ogura, Y., 1963: A review of numerical modeling research on small scale convection in the atmosphere. Meteorological Monographs, Vol. 5, No. 27, Severe Local Storms, pp. 65-75.

Orville, H.D., 1964: On mountain upslope winds. J. Atmospheric Sci., 21, pp. 622-633.

_____, 1965: A numerical study of the initiation of cumulus clouds over mountainous terrain. J. Atmospheric Sci., 22, pp. 684-699.

Orville, H.D., 1968: Ambient wind effects on the initiation and development of cumulus clouds over mountains. J. Atmospheric Sci., 25, pp. 385-403.

Penner, C.M., 1955: A three front model for synoptic analysis. Quart. J. Roy. Meteor. Soc., 81, pp. 89-91.

Petterssen, S., 1956: Weather analysis and forecasting. Vol. 2, 2nd ed., McGraw-Hill Book Co., N.Y., 266 pp.

Plate, E.J., 1971: Aerodynamic characteristics of the atmospheric boundary layer. United States Atomic Energy Commission, 190 pp.

Priestley, C.H.B., 1959: Turbulent transfer in the lower atmosphere. The University of Chicago Press, Chicago, 116 pp.

_____, and Taylor, R.J., 1972: On the assessment of surface heat flux and evaporation using large scale parameters. Mon. Wea. Rev., 100, pp. 81-92.

Reinelt, E.R., 1969-70: On the role of orography in the precipitation regime of Alberta. The Albertan Geographer, 6, pp. 45-58.

_____, 1973: On the synoptic climatology of migrant arctic highs in the Great Plains region. Department of Meteorology, Univ. of Oklahoma, Norman, Oklahoma, 94 pp.

Sawyer, J.S., 1959: The introduction of the effects of topography into methods of numerical forecasting. Quart. J. Roy. Meteor. Soc., 85, pp. 31-43.

Stewart, J.B., 1964: Precipitation from layer clouds. Quart. J. Roy. Meteor. Soc., 90, pp. 287-290.

Telford, J.W., and Warner, J., 1964: Fluxes of heat and vapour in the lower atmosphere derived from aircraft observations. J. Atmospheric Sci., 21, pp. 539-548.

Thompson, P.D., 1961: Numerical weather analysis and prediction. MacMillan and Co., N.Y., 166 pp.

Willet, H.C., and Sanders, F., 1959: Descriptive meteorology. Academic Press Inc., N.Y., 355 pp.

# APPENDIX

## BUILDING THE MODEL ATMOSPHERE

The model atmosphere was assumed to consist of three layers defined by distinctive lapse rates of potential temperature (see Fig. 3). The vertical structure of the model atmosphere was built up from surface parameters in the following manner:

(a) Calculation of temperature T and dewpoint temperature Td at the various levels in the vertical

(1) Level $Z_s$

$$T_s = T_o - [\gamma_s (Z_s - Z_o)]$$

where $\gamma_s = -\frac{\partial T}{\partial Z}$ was the superadiabatic lapse rate of temperature.

$$Td_s = Td_o - [\xi (Z_s - Z_o)]$$

where $\xi = -\frac{\partial Td}{\partial Z}$ was the lapse rate of dewpoint temperature.

(2) Levels $Z_m$ and h, where $Z_m = (Z_s + h)/2$

$$T = T_s - [\gamma (Z - Z_s)]$$

where $\gamma$ was the dry adiabatic lapse rate of temperature.

$$Td = Td_s - [\xi(Z - Z_o)]$$

(b) Calculation of equilibrium vapour pressures $e_o$, $e_s$, $e_h$ (dynes $cm^{-2}$) for levels $Z_o$, $Z_s$ and h using the Clausius-Clapeyron equation

$$e = 6.11 \times 10^3 \, EXP\left( \frac{L}{R_w} \left( \frac{1}{273} - \frac{1}{Td} \right) \right)$$

where L was the latent heat of evaporation assumed constant at the 0C value of 597.3 cal $gm^{-1}$. $R_w$ was the specific gas constant for water vapour.

(c) Calculation of the cloud base height or LCL

$$Z_{CB} = Z_o + \frac{T_o - Td_o}{\gamma - 0.17\gamma} \qquad \text{(Pettersen, 1956)}$$

where $Z_o$, $T_o$ and $Td_o$ were the initial values of terrain height, surface temperature, and dewpoint temperature.

(d) Calculation of the vertical mean of the horizontal pressure gradient

Pressure values at the various levels were needed to convert the temperature and vapour pressure values to potential temperature and specific humidity values. The vertical mean of the horizontal pressure gradient was obtained in terms of the norizontal wind which has been assumed constant with height. The somewhat arbitrary condition of balance between pressure gradient, Coriolis and friction forces was assumed at t = 0. Vertical homogeneity of the horizontal

wind implies that one pressure gradient applies at all levels. The pressure gradient is calculated by averaging the balanced equation of motion through the mixed layer, while neglecting the flux of momentum through the inversion surface which tops this homogeneous layer. Thus, the equation of motion becomes the Ekman balance equation:

$$0 = -\hat{k} \times f\vec{V} - \alpha\nabla p + \alpha \frac{\partial \vec{\tau}}{\partial Z}$$

With the assumptions outlined above and with $\vec{\tau}_s = C_D \rho |\vec{V}| \vec{V}$ the above equation becomes:

$$\alpha\nabla p = - \hat{k} \times f\vec{V} - \frac{C_D |\vec{V}| \vec{V}}{(h - Z_s)}$$

The pressure values at the various levels were then obtained in the following manner. $\alpha\nabla p$ calculated above was applied at level $Z_m$. Since density varies only slightly with pressure and an explicit value of pressure is required to integrate the above, it seemed quite sufficient to use the standard pressure height relationship based on the U.S. Standard Atmosphere to obtain first-guess pressure and density fields at level $Z_m$.

$$p_o = 1013.25 \left[1 - \frac{6.5 \times 10^{-5} Z_o}{288.16}\right]^{\frac{g}{6.5 \times 10^{-5} R}} \quad \text{dynes cm}^{-2}$$

$$p_s = p_o \left[1 - \frac{\gamma_s (Z_s - Z_o)}{T_o}\right]^{\frac{g}{\gamma_s R}} \quad \text{dynes cm}^{-2}$$

$$p_m = p_s \left[1 - \frac{\gamma (Z_m - Z_s)}{T_s}\right]^{\frac{g}{\gamma R}} \quad \text{dynes cm}^{-2}$$

and from the Equation of State

$$\alpha = \alpha_m = RT_m/p_m$$

The pressure field at level $Z_m$ was then given by:

$$p_m = p_{m1} + \frac{\partial p}{\partial x}\delta x + \frac{\partial p}{\partial y}\delta y$$

where $p_{m1}$ is the (1,1) grid point value of the first-guess pressure field. Because the above procedure gave pressures somewhat larger than expected on the basis of experience with the type of synoptic situation being considered, the value of $p_{m1}$ was reduced by about 1 percent before the integration was carried out. Pressure fields at levels $Z_o$, $Z_s$ and h were then calculated using the integrated form of the hydrostatic equation.

$$p_s = p_m \, EXP\left[\frac{g}{R\bar{T}_1}(Z_m - Z_s)\right]$$

where

$$\bar{T}_1 = (T_s + T_m)/2$$

$$p_o = p_s \, EXP\left[\frac{g}{R\bar{T}_2}(Z_s - Z_o)\right]$$

where

$$\bar{T}_2 = (T_o + T_s)/2$$

$$p_h = p_m \, EXP\left[\frac{g}{R\bar{T}_3}(Z_m - h)\right]$$

where

$$\bar{T}_3 = (T_m + T_h)/2$$

(e) Calculation of potential temperatures at levels $Z_o$, $Z_s$ and h

$$\theta = T\left[\frac{p_*}{p}\right]^{\kappa}$$

where $p_*$ is the reference level of 1000 mb and $\kappa = R/C_p$ with $C_p$ equal to the specific heat at constant pressure for dry air:

$$0.240 \text{ cal gm}^{-1} \text{ K}^{-1}.$$

(f) Calculation of specific humidity at levels $Z_o$, $Z_s$ and h

$$q = \frac{0.622e}{p - 0.378e}$$

(g) Calculation of mean mixed layer ($Z_s$ to h) values used to initialize the model

$$\theta = (\theta_s + \theta_h)/2$$

and

$$q = (q_s + q_h)/2.$$